The N-terminal domain of the Schaaf–Yang syndrome protein MAGEL2 likely has a role in RNA metabolism

Received for publication, March 26, 2021, and in revised form, June 22, 2021 Published, Papers in Press, July 12, 2021,
https://doi.org/10.1016/j.jbc.2021.100959

Matthea R. Sanderson[1], **Richard P. Fahlman**[2,3], **and Rachel Wevrick**[1,*]

From the [1]*Department of Medical Genetics,* [2]*Department of Biochemistry,* [3]*Department of Oncology, University of Alberta, Edmonton, Alberta, Canada*

Edited by Karin Musier-Forsyth

MAGEL2 **encodes the L2 member of the melanoma-associated antigen gene (MAGE) protein family, truncating mutations of which can cause Schaaf-Yang syndrome, an autism spectrum disorder.** ***MAGEL2*** **is also inactivated in Prader–Willi syndrome, which overlaps clinically and mechanistically with Schaaf–Yang syndrome. Studies to date have only investigated the C-terminal portion of the** ***MAGEL2*** **protein, containing the MAGE homology domain that interacts with RING-E3 ubiquitin ligases and deubiquitinases to form protein complexes that modify protein ubiquitination. In contrast, the N-terminal portion of the MAGEL2 protein has never been studied. Here, we find that MAGEL2 has a low-complexity intrinsically disordered N-terminus rich in Pro-X_n-Gly motifs that is predicted to mediate liquid–liquid phase separation to form biomolecular condensates. We used proximity-dependent biotin identification (BioID) and liquid chromatography–tandem mass spectrometry to identify MAGEL2-proximal proteins, then clustered these proteins into functional networks. We determined that coding mutations analogous to disruptive mutations in other MAGE proteins alter these networks in biologically relevant ways. Proteins identified as proximal to the N-terminal portion of MAGEL2 are primarily involved in mRNA metabolic processes and include three mRNA N 6-methyladenosine (m^6A)-binding YTHDF proteins and two RNA interference-mediating TNRC6 proteins. We found that YTHDF2 coimmunoprecipitates with MAGEL2, and coexpression of MAGEL2 reduces the nuclear accumulation of YTHDF2 after heat shock. We suggest that the N-terminal region of MAGEL2 may have a role in RNA metabolism and in particular the regulation of mRNAs modified by m^6A methylation. These results provide mechanistic insight into pathogenic** ***MAGEL2*** **mutations associated with Schaaf–Yang syndrome and related disorders.**

MAGEL2 encodes the L2 member of the melanoma-associated antigen gene (MAGE) protein family. Like the 34 other MAGE proteins, MAGEL2 contains a conserved MAGE homology domain (MHD) (1). MAGE proteins regulate protein ubiquitination, through interactions between the MHD and variable domains of E3 ubiquitin ligases and deubiquitinases, to form MAGE-RING E3 ligase complexes that serve as multifunctional hubs for the modification of key substrates in the cell (2–4). MAGEL2 regulates the vesicular and endosomal trafficking of membrane-bound receptors and also regulates the stability of proteins important for nuclear-cytoplasmic trafficking, cilia, and other cellular activities (5–10). However, functional studies have assessed only a truncated version of the MAGEL2 protein that contains the C-terminally located MHD but not the N-terminal portion of the protein (6–8, 11–15). Despite a growing body of evidence supporting a critical role for MAGEL2 in development and physiology, there is still little known about its cellular role and in particular the role of the N-terminal portion of MAGEL2.

Missense, frameshift, or nonsense mutations in six of the 35 MAGE genes cause genetic disorders: *MAGED2* is mutated in Bartter syndrome (16), *NSMCE3* (*MAGEG1*) in lung disease, immunodeficiency, and chromosome breakage syndrome (17), *MAGEA9* and *MAGEB4* in cases of male infertility (18–20), while *MAGEA6* mutations promote pancreatic cancer initiation and progression (21, 22). *De novo* or paternally inherited protein-truncating mutations in *MAGEL2* cause MAGEL2-related disorders (Schaaf–Yang syndrome, SYS) (23, 24). Infants with SYS typically present with developmental delay, feeding problems, hypotonia, and joint contractures (25, 26), followed in childhood by intellectual disability, autism spectrum disorder, and endocrine dysfunction (27, 28). Children with SYS have initially been diagnosed with severe hypotonia with respiratory distress (26), recurrent fetal malformations (29), arthrogryposis multiplex congenita, and endocrine dysfunction (30), Chitayat–Hall syndrome (distal arthrogryposis, intellectual disability, dysmorphic features, and hypopituitarism) (31), Crisponi/cold-induced sweating syndrome (hyperthermia, camptodactyly, feeding and respiratory difficulties, scoliosis) (32), hypotonia/obesity syndrome (33), or Opitz trigonocephaly-C (34). A perinatal lethal phenotype is associated with a specific MAGEL2 mutation (c.1996delC, p.Q666Sfs*36), and moderate to severe phenotypes are associated with the reciprocal mutation, c.1996dupC (p.Q666Pfs*47, found in 40% of cases) (26–29, 31, 34–39). More moderate SYS phenotypes are associated with 39 different protein-truncating mutations located elsewhere in *MAGEL2* (27, 28). As a single exon gene, stop or frameshift mutations in MAGEL2 are not predicted to cause nonsense-

* For correspondence: Rachel Wevrick, rwevrick@ualberta.ca.

mediated RNA decay, and mutant MAGEL2 RNA has been detected at a low level in a human fetus carrying p.Q666Sfs*36 (37). The *MAGEL2* gene is in the microdeletion region associated with Prader–Willi syndrome (PWS), a neurodevelopmental disorder phenotypically similar to SYS (24).

Missense mutations in MAGE proteins may disrupt protein–protein interactions and function. Mutations in MAGEL2 impair its ability to facilitate retromer-dependent recycling of proteins from endosomes back to the *trans*-Golgi network, to promote the cell surface expression of the leptin receptor and to regulate the ubiquitination and stability of the circadian rhythm protein CRY1 (7–9). MAGEL2 is most highly expressed in the hypothalamus and to a lesser extent in other regions of the brain and also in the developing musculoskeletal system. Studies in mice also support a critical role for MAGEL2 in the normal development and function of the nervous and endocrine systems, muscle, and bone. Mice carrying paternally inherited *Magel2* mutations have phenotypes reminiscent of SYS, including pre- and perinatal lethality, behavioral abnormalities, abnormal body composition, endocrine dysfunction, low muscle tone, and scoliosis (5, 40–52).

In this study, we identified proteins in proximity to either the C-terminal portion of MAGEL2 or the entire MAGEL2 protein using *in vivo* proximity-dependent biotin identification (BioID) and affinity capture coupled to liquid chromatography–tandem mass spectrometry (LC-MS/MS) in cultured human cells. We examined how amino acid substitutions in the MHD alter the set of proteins in proximity to MAGEL2, demonstrating the potential utility of protein–protein proximity mapping for the assessment of *MAGEL2* variants of unknown significance in individuals clinically suspected to have SYS. Our study suggests that the N-terminus of MAGEL2 contains an intrinsically disordered domain and associates with proteins that function in mRNA metabolism and cellular stress responses. These results could shed light on the phenotypes associated with both PWS, where there is complete loss of MAGEL2, and SYS, where affected individuals may produce mutant or partial MAGEL2 proteins.

Results

Annotation of MAGEL2 functional domains and features

The *MAGEL2* gene was originally predicted to encode a 529 amino acid protein containing a conserved MAGE homology domain (MHD, pfam01454). The DNA upstream of the predicted start codon contains multiple repeated sequences that at the time were not present in cDNA libraries and were refractory to RT-PCR, so this region was assumed to be part of the 5′ untranslated region (11, 53). More recent genome annotation suggests that human MAGEL2 encodes a protein of 1249 amino acid (aa) residues with the MHD from residues 1027 to 1195 (2, 11, 53, 54) (UniProt Q9UJ55) (Fig. 1). A second protein motif, also in the C-terminal portion of MAGEL2, was experimentally determined: U7B, from aa 820 to 1034, binds to the TRAF domain of the ubiquitin-specific protease USP7 (8). We used the NCBI Conserved Domain Database (CDD v.3.17) to analyze MAGEL2 protein. The MHD was a specific hit, representing very high confidence that the query sequence belongs to the same protein family as the sequences used to create the domain model (55). CDD identified seven "non-specific" domains as hits, all of which exceed the default threshold for statistical significance. The portion of MAGEL2 N-terminal to U7B (aa 1–819) is rich in proline (28%), alanine (15%), and glutamine (11%) residues and is predicted to be basic (theoretical isoelectric point 11.5). The N-terminal portion contains two PHA03247 domains, which are low complexity regions rich in alanine, proline, and serine residues (56). CDD also identified a Atrophin-1 domain that contains a polyglutamine repeat (57), a topoisomerase II-associated PAT1 domain (58), a PRK14951 region that is shared with the DNA polymerase III subunits gamma and tau, a PABP-1234 region that is shared among the mRNA-binding PABP proteins, and a PcoB domain, which is present in proteins involved in copper transport. The unusual amino acid composition of the N-terminal region contributes to its predicted instability: its "instability index" is computed to be 79, where a protein whose instability index is ≤40 is predicted as stable (59).

Intrinsically disordered protein regions contain stretches of ≥30 disorder-promoting residues (Arg, Pro, Gln, Gly, Glu, Ser, Ala, and Lys). Using SPOT-Disorder2 (60), we found that about 85% of the MAGEL2 protein, including the entire N-terminal region and a short segment at the extreme C-terminus, exceeds the threshold for an intrinsically disordered protein region (Fig. 1*A*). MAGEL2 is thus one of the 14.5% of human proteins that contain a folded domain (*i.e.*, the MAGE homology domain) and in which intrinsically disordered regions constitute half or more of the protein (61). Intrinsically disordered proteins that are rich in proline and glycine can undergo phase transitions that mediate self-assembly events; examples include elastin-like and collagen-like proteins (61, 62). Protein segments containing proline-glycine pairs separated by up to four residues (P-X_n-G, where X is any residue), with these motifs separated by 3 to 15 residues, form scaffolds for intrinsically disordered protein polymers. The P-G dipeptide is the predominant motif in these proteins. The N-terminal portion of MAGEL2 is rich in P-X_n-G motifs, with the portion of MAGEL2 N-terminal to U7B containing 24 P-G dipeptides and 13 other P-X_n-G motifs (Fig. 1 and Fig. S1*A*). The first 16 P-G dipeptides each start a repeating decapeptide with a consensus sequence approximating P-G-T/V/A-P-M-A/V-H/Q-P-P-P from aa 105 to 263, overlapping the RNA recognition motif (PFAM 00076) of the PABP-1234 domain (63). The average spacing of the P-X_n-G motifs in the N-terminal portion of MAGEL2 is 15, at the upper end of the range for motifs that form scaffolds for intrinsically disordered protein polymers. Another repeating structure wherein 14 P-P dipeptides each start a repeating heptapeptide with a consensus sequence approximating P-P-P/V/L-I-R-Q-A spans from aa 405 to 502. These repeating proline-rich structures may form scaffolds for intrinsically disordered MAGEL2 polymers (model in Fig. S1*B*). We quantified the propensity of MAGEL2 to contribute to phase separation. MAGEL2 had an overall P-Score of 4.66 using the P-score predictor algorithm,

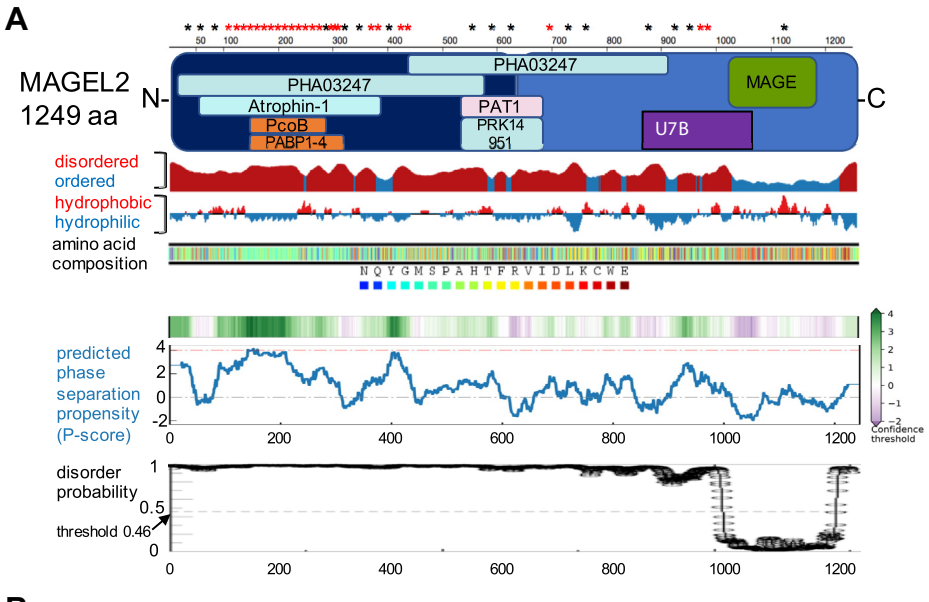

B

Motif	Accession	Description	Interval	E-value
MAGE	pfam01454	The MAGE (melanoma antigen-encoding gene) family are expressed in a wide variety of tumors but not in normal cells, with the exception of the male germ cells, placenta, and, possibly, cells of the developing embryo.	1027-1195	6.93E-25
PHA03247	PHA03247	large tegument protein UL36; Provisional	9-576	1.29E-21
Atrophin-1	pfam03154	Atrophin-1 family. Atrophin-1 is the protein product of the dentatorubral-pallidoluysian atrophy (DRPLA) gene.	50-387	3.69E-11
PAT1	pfam09770	Topoisomerase II-associated protein PAT1. Members of this family are necessary for accurate chromosome transmission during cell division.	532-683	1.56E-08
PHA03247	PHA03247	large tegument protein UL36; Provisional	434-913	1.15E-07
PRK14951	PRK14951	DNA polymerase III subunits gamma and tau; Provisional	532-683	8.79E-07
PABP-1234	TIGR01628	polyadenylate binding protein, human types 1, 2, 3, 4 family; These eukaryotic proteins recognize the poly-A of mRNA and consists of four tandem RNA recognition domains at the N-terminus (rrm: pfam00076) followed by a PABP-specific domain (pfam00658) at the C-terminus. The protein is involved in the transport of mRNA's from the nucleus to the cytoplasm.	117-256	1.60E-05
PcoB	COG3667	Uncharacterized protein involved in copper resistance [Inorganic ion transport and metabolism]	119-224	4.52E-04

Figure 1. Analysis of domains and features in the human full-length MAGEL2 protein. *A*, diagram of human MAGEL2 protein (UniProt Q9UJ55) showing location of protein domains and predicted protein structure. Locations of P-G dinucleotides (**red*) and P-Xn-G motifs (**black*) are indicated at the *top*. Disordered *versus* ordered regions are shown in *red* (potentially disordered region), *blue* (probably ordered region). Hydropathy has been calculated using a sliding window of 15 residues and summing up scores from standard hydrophobicity tables. *Red*: hydrophobic, *Blue*: hydrophilic, adapted from Protein Data Bank: https://www.rcsb.org. Predicted phase separation propensities (PScore) are shown below. A score greater than 4 is considered a confident phase separation prediction and a score of 0 represents the Protein Data Bank average. *B*, domains were predicted by CDD, except for the USP7 binding domain (U7B), which was experimentally determined.

whereby a score ≥4 is considered a confident phase separation prediction, and a score of 0 is average for all proteins in the Protein Data Bank (64). Such low-complexity intrinsically disordered regions can mediate liquid–liquid phase separations to form biomolecular condensates, such as stress granules and P-bodies. As well, proteins associated with autism and neurological disorders are more likely to have higher P-scores than other proteins in the human proteome (61).

Strategy to identify proteins in proximity to MAGEL2

We and others previously identified proteins that interact with a C-terminally truncated version of MAGEL2 by yeast two-hybrid screens, affinity capture western, and a mammalian two-hybrid technique called MAPPIT (6–8, 65, 66). Collectively, these studies identified 12 human and five mouse proteins that interact with the C-terminal portion of MAGEL2 (Table S1). Consistent with functional studies of MAGEL2, the interacting proteins are involved in biological processes such as Arp2/3 complex-mediated actin nucleation, protein K63-linked ubiquitination, and endosome to Golgi retrograde transport. We designed a strategy to identify physiologically relevant proteins in proximity to the entire MAGEL2 protein or to the C-terminal portion, reasoning that we could compare these sets of proteins to implicitly identify proteins in proximity to the unstudied N-terminal portion of MAGEL2. HEK293 Flp-In T-REx cells were stably transfected with a 3xFLAG epitope-tagged-BirA* biotin ligase fused in frame to the N-terminus of either the C-terminal 645 residues of the *MAGEL2* open reading frame or to the entire *MAGEL2* open reading frame, creating HEK293-CtermMAGEL2 and HEK293-MAGEL2 cells respectively (Fig. 2*A*). The FLAG-BirA* constructs integrate as a single copy into a defined site in the HEK293 Flp-In T-REx genome, and protein expression is inducible with tetracycline in the stable cell line (67, 68). Immunoblotting of lysates from tetracycline-induced cells confirmed the expression of the FLAG-BirA* fusion proteins at the expected molecular weight (Fig. 2*B*). The presence of recombinant FLAG-BirA*-tagged proteins in the cytoplasm of induced cells was detected by indirect immunofluorescence microscopy, consistent with the cytoplasmic localization of endogenous MAGEL2 protein (7, 25) (Fig. 2*C*).

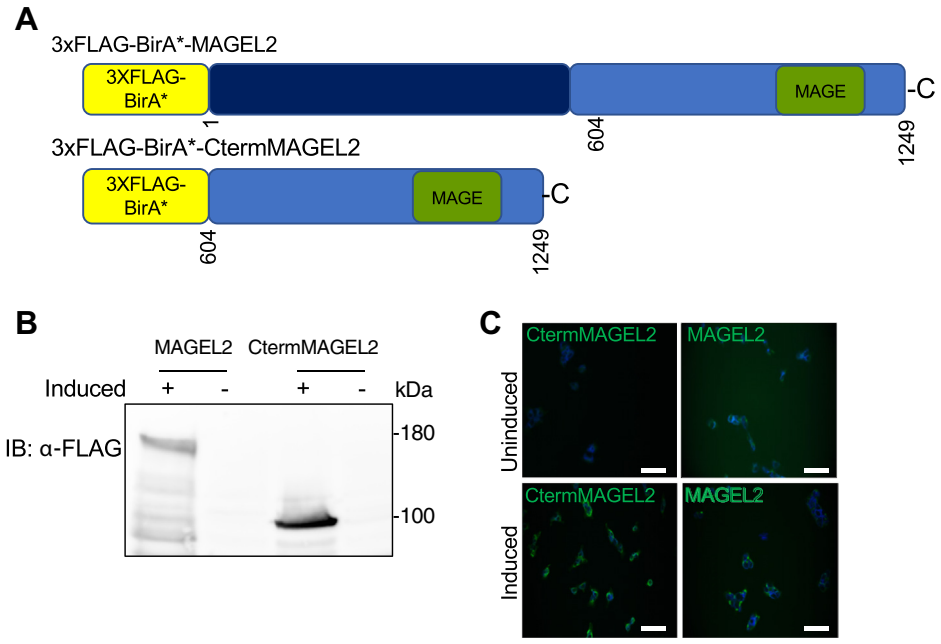

Figure 2. Generation and expression of BirA*-MAGEL2 constructs. *A*, a 3XFLAG epitope tag and BirA* biotin ligase were fused in frame with the entire 1249 amino acids of MAGEL2 open reading frame or 645 amino acids of the C-terminal end of the MAGEL2 open reading frame. *B*, stably transfected HEK293 cell lines express MAGEL2 when induced with tetracycline. FLAG-BirA*-MAGEL2 (MAGEL2) and FLAG-BirA*-CtermMAGEL2 (CtermMAGEL2) proteins were detected in protein lysates from stably transfected HEK293 Flp-In cells induced with tetracycline (+) or not (–) by immunoblotting with anti-FLAG antibodies. *C*, expression of FLAG-BirA*-MAGEL2 in stably transfected and tetracycline-induced HEK293-MAGEL2 cells plated on coverslips, visualized using anti-FLAG antibodies and confocal microscopy (*green*). Nuclei were counterstained *blue* with Hoechst. Scale bar 50 μm.

Functional and Gene Ontology (GO) analyses of CtermMAGEL2 proximal proteins revealed putative MAGEL2 complexes

Expression of FLAG-BirA*-CtermMAGEL2 was induced in HEK293-CtermMAGEL2 cells cultured in excess biotin. Biotinylated proteins were affinity-purified from cell lysates, processed by tryptic digestion, and analyzed by LC-MS/MS (69). We detected 108 biotinylated proteins that are predicted to have passed within 10 nm of FLAG-BirA*-CtermMAGEL2 (Table S2). We retained proteins found in at least three of six biological replicate samples and not present at high levels in a contaminant repository for affinity purification–mass spectrometry data (CRAPome, see Experimental procedures) (70). After data processing, 44 CtermMAGEL2-proximal proteins were identified (Table S2). One protein, USP7, had been previously identified as a CtermMAGEL2 interactor by tandem affinity purification and coimmunoprecipitation, while the other proteins were not previously associated with MAGEL2 (8, 9). While we consider these to be potential C-terminal interacting proteins, it is also possible that the N-terminal protein of MAGEL2 could alter the conformation of the C-terminal portion of the protein and influence recruitment of its binding partners.

We investigated whether physical interactions among any of the 44 CtermMAGEL2-proximal proteins had been previously detected, using the online tool "STRING: Functional protein association networks" to seed the analysis (71). We did not consider interactions that were based solely on text-mining or coexpression data, focusing on physical interactions, identifying six clusters of CtermMAGEL2-proximal proteins (Fig. 3). Clusters 1 and 2 contain RNA metabolism and translation initiation proteins. Cluster 1 proteins DHX9, YBX1, and HNRNPU associate with IGF2BP1, which binds to the coding

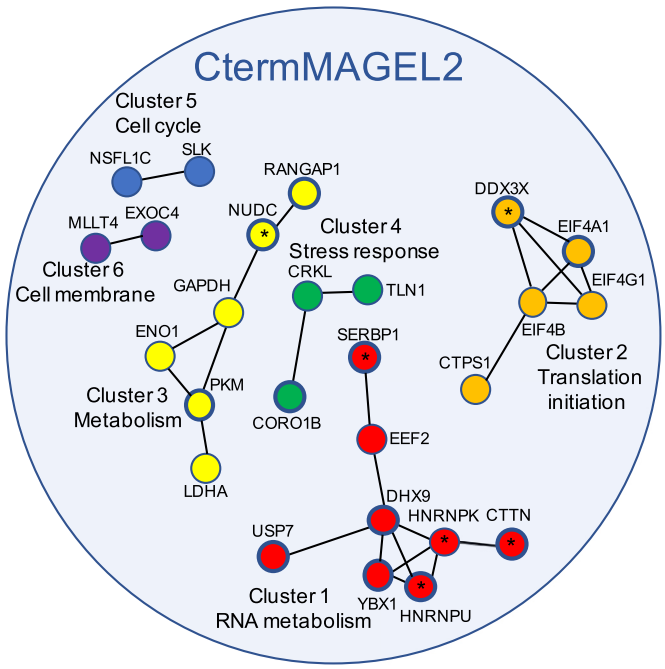

Figure 3. STRING analysis of proteins in proximity to CtermMAGEL2 as detected by BioID-MS. The 44 CtermMAGEL2-proximal proteins participate in six clusters of interacting proteins. Proteins later identified as also proximal to the full-length MAGEL2 protein are indicated with a *star*. Proteins with *thicker outlines* were found in all six BioID replicates.

region instability determinant of mRNAs and regulates their stability (72). Cluster 2 includes mRNA-binding proteins: eukaryotic initiation factors eIF4A1, eIF4B, and eIF4G are required for the recruitment of the small 40S ribosomal subunit along with other factors that make up the 43S preinitiation complex in preparation for scanning to the AUG codon (73, 74). These eIF proteins interact with DDX3X, a DEAD-box helicase that can substitute for eIF4E in the eukaryotic initiation complex (75). eIF proteins are also components of stress granules (75). Cluster 3 includes the glycolysis proteins GAPDH, ENO1, PKM, and LDHA (76, 77). Cluster 4 is composed of three cellular signaling proteins: CRK-like protein (CRKL), coronin 1B (CORO1B), and talin-1 (TLN1) (78–80). Cluster 5 proteins regulate the cell cycle: STE20-like kinase (SLK) mediates apoptosis and actin stress fiber dissolution (81), while NSFL1 cofactor p47 (NSFL1C) is important for fragmentation and reassembly of Golgi stacks during cell division (82). Finally, Cluster 6 proteins adafin (MLLT4/ADFN) and exocyst complex component 4 (EXOC4) are PDZ domain-containing proteins that facilitate the formation of cell–cell junctions and docking of vesicles at the cell membrane respectively (83, 84). We next examined whether biological processes or molecular function pathways were enriched among CtermMAGEL2-proximal proteins, using GO algorithms in Cytoscape app (85) (Table S3). As expected, GO classifications mirrored the cores of clusters that were identified by protein–protein interaction analyses in STRING. The category with the most proteins was cadherin binding, followed by ribonucleoprotein complex binding, including subheadings related to translation initiation as well as RNA binding and processing.

Amino acid substitutions in the MAGE homology domain alter the proximity of proteins to the C-terminal portion of MAGEL2

Mutations in MAGE proteins can disrupt their function, in part because of changes to protein–protein interactions (8, 17). We examined whether CtermMAGEL2 proteins carrying amino acid substitutions in the MHD have different proximal proteins compared with wild-type CtermMAGEL2. Two mutant FLAG-BirA*-CtermMAGEL2 cDNA constructs were generated by site-directed mutagenesis, then stably transfected into HEK293 Flp-In T-Rex cells to generate cell lines that are isogenic to the wild-type FLAG-BirA*-CtermMAGEL2 cell line except for the presence of the engineered mutation (Fig. S2*A*). CtermMAGEL2p.R1187C was modeled on a pathogenic missense mutation in a highly conserved arginine residue in the second of two tandem winged helix motifs (WH-B) in the MHD of MAGED2 identified in a patient with Bartter syndrome (4, 16). Mutations in the WH-B of NSMCE3 (MAGEG1) disrupt its ability to bind to double-stranded DNA (86, 87). The double substitution CtermMAGEL2p.LL1031AA (in the WH-A motif) is analogous to engineered mutations in the MAGEG1/NSMCE3 protein that disrupt its ability to bind to the RING-type E3 ubiquitin ligase NSE1 (4, 17). Both MAGEL2 mutations are predicted to alter the structure of the MHD when analyzed using bioinformatic tools (88). These mutations also interfere with MAGEL2 function in ubiquitination assays (7, 9). Induced expression and cytoplasmic localization of each mutant FLAG-BirA*-CtermMAGEL2 protein were substantiated by immunoblotting of cell lysates (Fig. S2*B*) and immunofluorescence microscopy of tetracycline-induced cells (Fig. S2*C*).

Proteins in proximity to CtermMAGEL2p.LL1031AA and CtermMAGEL2p.R1187C were identified by BioID-LC-MS/MS and removal of background proteins, then compared with the set of proteins proximal to wild-type CtermMAGEL2. We defined "lost" interactions as those not detected in any of the three replicates with a mutant CtermMAGEL2 but detected in at least three of six wild-type CtermMAGEL2 replicates, whereas a "gain" of interaction was a proximal protein present in all three replicates for mutant CtermMAGEL2 protein but absent from all six wild-type replicates. Using these definitions, CtermMAGEL2p.LL1031AA had 19 fewer proximal proteins and CtermMAGEL2p.R1187C had six fewer proximal proteins than wild-type CtermMAGEL2 (Fig. 4*A*, Table S2), but CtermMAGEL2p.LL1031AA gained two proximal proteins and CtermMAGEL2p.R1187C gained 12 proximal proteins compared with wild-type CtermMAGEL2 (Fig. 4*B*, Table S2). These results suggest that amino substitutions in the MHD modify the complement of proteins in proximity to MAGEL2. Lastly, nine proteins were proximal to MAGEL2 in all six replicates of the wild-type protein, all three CtermMAGEL2p.LL1031AA replicates, and all three CtermMAGEL2p.R1187C replicates, so represent proximal

A

LOST	Cterm MAGEL2	p.LL1031AA	p.R1187C
NSFL1C	P	P	A
CKB	P	A	P
CRKL	P	A	P
CTPS1	P	A	P
DHX9	P	A	P
EEF2	P	A	P
EPB41L3	P	A	P
EXOC4	P	A	P
GCN1	P	A	P
IFIT5	P	A	P
LARP1	P	A	P
MRE11A	P	A	P
NONO	P	A	P
PCM1	P	A	P
TLN1	P	A	P
AHCY	P	A	A
ENO1	P	A	A
LDHA	P	A	A
POTEF	P	A	A
YBX1	P	A	A

B

GAINED	Cterm MAGEL2	p.LL1031AA	p.R1187C
CEP170	A	P	P
PDAP1	A	P	P
ANKHD1	A	A	P
ATXN2L	A	A	P
CKAP5	A	A	P
EIF5	A	A	P
HCFC1	A	A	P
IRS4	A	A	P
PCBP2	A	A	P
PDLIM5	A	A	P
SRP68	A	A	P
UBE2O	A	A	P

C

ALL REPLICATES	Cterm MAGEL2	p.LL1031AA	p.R1187C
NUDC	P	P	P
EIF4A1	P	P	P
CTTN	P	P	P
USP7	P	P	P
CORO1B	P	P	P
RANGAP1	P	P	P
GIGYF2	P	P	P
PKM	P	P	P
SERBP1	P	P	P
HNRNPU	P	P	P
DDX3X	P	P	P

Figure 4. CtermMAGEL2 proteins carrying amino acid substitutions have losses and gains of proximal proteins compared with wild-type CtermMAGEL2. *A*, proteins present (P) in at least three out of six replicates of BioID-MS with the wild-type CtermMAGEL2 protein but absent (A) in all three replicates of BioID-MS with the mutant CtermMAGEL2 protein are listed. *B*, proteins absent (A) in six out of six replicates of BioID-MS with the wild-type CtermMAGEL2 protein but present (P) in all three replicates with either of the mutant CtermMAGEL2 proteins are listed. *C*, proteins present (P) in all six replicates of the wild-type protein, all three CtermMAGEL2p.LL1031AA replicates, and all three CtermMAGEL2p.R1187C replicates.

proteins that are insensitive to these missense mutations in the MAGE homology domain (Fig. 4*C*, Table S2). Six of these proteins are involved in RNA metabolism or translation initiation.

We used STRING to find previously identified interactions among proteins proximal to the two mutant CtermMAGEL2 proteins. Four clusters of proteins were proximal to CtermMAGEL2p.LL1031AA (Fig. S3), while the CtermMAGEL2p.R1187C proximal proteins formed five clusters (Fig. S4). Both mutant proteins maintained interactions with the glycolytic cluster of proteins identified as proximal to wild-type CtermMAGEL2, as well as many of the mRNA binding proteins. However, both MAGEL2 proteins carrying MHD mutations lost interactions with the coding region instability determinant binding proteins YBX1 and DHX9. CtermMAGEL2p.R1187C protein is still proximal to other members of the mRNA-binding core in Cluster 2 containing the proteins eIF4A1, eIF4B, eIF4G1, and DDX3X, while CtermMAGEL2p.LL1031AA maintained proximity to fewer proteins in this cluster. CtermMAGEL2p.R1187C is proximal to more proteins involved in cellular stress response. The CtermMAGEL2p.R1187C Cluster 4 is an expansion of wild-type Cluster 4, with the addition of the adaptor protein crk (CRK). IRS4 is the only member of this cluster not associated with cellular stress response. However, IRS4 is involved in cellular signaling, linking it with the proteins CRK and CRKL (89, 90).

The full-length MAGEL2 protein interactome is enriched in proteins important for mRNA metabolism

MAGEL2 encodes a 1249 amino acid protein. However, cellular studies to date have only examined truncated recombinant proteins containing the C-terminal half of MAGEL2 (6–9, 13–15). To initiate investigation of the N-terminal portion of MAGEL2, we used BioID to identify proteins in proximity to the full-length MAGEL2 protein. Comparing these full-length MAGEL2 proximal proteins to proteins proximal to the C-terminal portion implicitly identifies proteins proximal to the unstudied N-terminal portion of MAGEL2. Expression of FLAG-BirA*-MAGEL2 (*i.e.*, full length) was induced in HEK293-MAGEL2 cells cultured in excess biotin, and 34 proximal proteins were identified by BioID-LC-MS/MS and elimination of contaminants (Table S2). These MAGEL2-proximal proteins form eight clusters of proteins by STRING analysis (Clusters A–H, Fig. 5*A*). Cluster A contains a set of RNA binding and processing proteins, including polyadenylate-binding protein 1 (PABPC1), a protein that binds to the poly (A) tail of mRNA and regulates it through splicing and stability (91, 92). Other proteins in Cluster A are also involved in mRNA metabolism: CSDE1, DDX3X, HNRNPK, HNRNPU, TNRC6A, TNRC6B, SERBP1, and ZFR (93–98). Cluster B is made up of Ubiquitin-associated protein 2-like (UBAP2L), proline-rich coiled-coil 2 A (PRRC2A) and PRRC2C, which bind and process RNA and are core stress granule proteins (99, 100) PRRC2A is also a m^{6}A reader protein (101). N^6-methyladenosine (m^{6}A) is the most common eukaryotic mRNA modification, and m^{6}A RNA

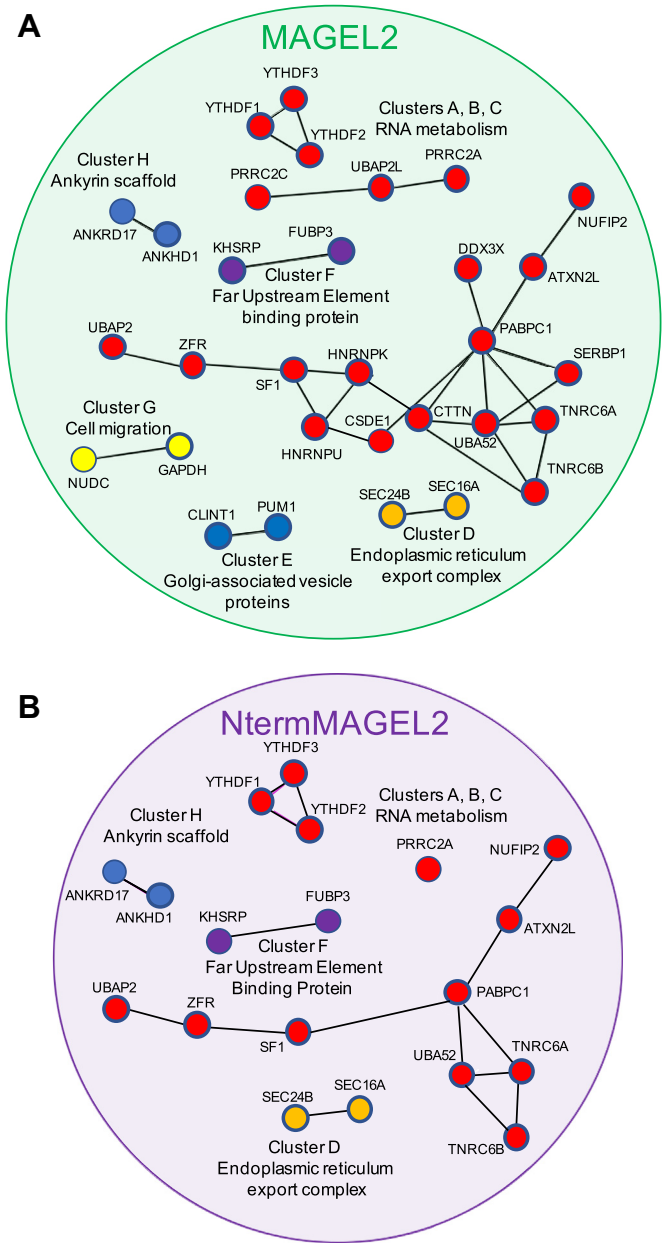

Figure 5. Protein–protein interaction analysis of proteins in proximity to MAGEL2 as detected by BioID-MS. *A*, the 34 proteins identified in at least two out of three replicate BioID-MS experiments with MAGEL2 and not eliminated as background contaminating proteins were analyzed. Interactions among MAGEL2-proximal proteins were identified, revealing eight clusters of proteins. Proteins outlined with *thicker lines* were found in three out of three replicates. *B*, interactions among proteins proximal to full-length MAGEL2 but not CtermMAGEL2 and deduced to be proximal to the N-terminal, intrinsically disordered portion of MAGEL2. Proteins found in all three replicates of the BioID for full-length MAGEL2 and none of the replicates for C-terminal MAGEL2 are outlined with *thicker lines*.

modification is recognized and bound by reader proteins that regulate mRNA stability and the rate of mRNA translational output (102, 103). Regulation of m^{6}A dependent processes is important for neurogenesis and synaptic function, and dysregulation occurs in disorders such as Fragile X syndrome. Cluster C has YTHDF1, YTHDF2, and YTHDF3 (YT521-B homology Containing Family 1/2/3), which are important for the translation and degradation of m^{6}A modified mRNAs (102,

104, 105). In Cluster D, SEC16A and SEC24B function in export of cargo from the endoplasmic reticulum (106–108). PUM1 (Pumilio homolog 1) and CLINT1 (Clathrin interactor 1) are Golgi-associated vesicle interacting proteins that form Cluster E (109). PUM1 binds to mRNA and directs it to be repressed or translated (110), and CLINT1 plays a role in clathrin-coated vesicles from the *trans*-Golgi network (111). FUBP3 and KHSRP (FUBP2) are far upstream element (FUSE) binding proteins that bind RNA and single-stranded DNA and form Cluster F. In Cluster G, the chaperone protein (NUDC) plays a role in neuronal cell migration (112), while glyceraldehyde-3-phosphate dehydrogenase (GAPDH) is a metabolic protein. Cluster H contains ankyrin scaffold proteins ANKHD1 and ANKRD17, which regulate nucleocytoplasmic trafficking of the transcriptional regulator YAP and cytokine receptor signaling.

The full-length MAGEL2 interactome contains proteins that are not in the C-terminal MAGEL2 interactome and are inferred to be proximal to the N-terminal portion of MAGEL2

Ideally, we would next identify proteins in proximity to the N-terminal region of the MAGEL2 protein, expressed without the C-terminal region. However, this experiment is complicated by the unusual amino acid composition of the N-terminal region that renders it prone to aggregation, unstable, and likely to mislocalize in the cell. Instead, we compared the 34 proteins proximal to full-length MAGEL2 to the 44 proteins proximal to the C-terminal portion of MAGEL2, identifying 12 proteins common to both datasets and inferred to be proximal to C-terminal MAGEL2. There were 22 proteins new to the full-length MAGEL2 interactome and not found in any of the six replicate BioID experiments with C-terminal MAGEL2, suggesting that these proteins are in proximity to the N-terminal portion of MAGEL2 (Fig. 5*B*, Fig. S5, Table S4). Alternatively, some of these proteins could be proximal to the C-terminal region of MAGEL2 only when the N-terminal region is present, as a result of a change in conformation or subcellular localization. Functional pathways enriched among presumed N-termMAGEL2 proximal proteins were identified using associated GO terms (85) (Table S5). Nineteen of the 22 proteins are involved in transcription or mRNA processing, including many that interact with each other (Fig. 5). TNRC6A and TNRC6B and YTHDF1, YTHDF2, and YTHDF3 are RNA-binding proteins (104, 113). PABPC1 (polyadenylate-binding protein C1) is one of several PABP proteins that have roles in RNA metabolic pathways, including recognition of poly(A) tails of mRNAs and mRNA transport from the nucleus to the cytoplasm (114). PABPC1 also binds TNRC6A (115). Interestingly, the N-terminal portion of MAGEL2 itself contains a PABP domain, between residues 117 and 256, suggesting that the MAGEL2 N-terminal domain may function as a PABP-like protein.

YTHDF2 was proximal to MAGEL2 in all three replicate BioID experiments. A previous comprehensive study of mRNA-associated processes or complexes by BioID proximity mapping identified 100 proteins as high-confidence interactors of YTHDF2 (100, 104). Of the 22 proteins deduced to be in proximity to the N-terminal portion of MAGEL2, 14 were among the 100 high-confidence YTHDF2 interactors (Fig. S6). As well, 13 of these proteins are among the top 25 interactors for the set of YTHDF1, YTHDF2, and YTHDF3 proteins (104). MAGEL2 is not endogenously expressed in HEK293 cells used for BioID, so was not identified as a YTHDF interactor. However, the MAGE family member MAGED1 was one of the top 100 YTHDF2 interacting proteins (Fig. S6). This observation, and the fact that mRNA-binding proteins are also enriched in the interactome of necdin, a highly related MAGE protein (88), raises the possibility that MAGE proteins MAGEL2, necdin, and MAGED1 might serve redundant roles in mRNA-associated complexes.

MAGEL2 complexes with YTHDF proteins, and YTHDF2 levels are reduced in PWS fibroblasts

The C-terminal portion of MAGEL2 is an adaptor for protein ubiquitination, a posttranslational modification that alters protein stability (6, 7, 9). YTHDF2 undergoes ubiquitin-mediated proteolysis in a cell-cycle-dependent manner (116). In a cotransfection experiment, we found that coexpression of MAGEL2 increased the steady-state levels of YTHDF2 (Fig. S7). Moreover, we found less endogenous YTHDF2 protein in fibroblasts derived from individuals with PWS, who lack MAGEL2, *versus* control fibroblasts (Fig. 6*A*). Next, given that BirA*-MAGEL2 proximity labels YTHDF1, YTHDF2, and YTHDF3, MAGEL2 and YTHDF proteins may be near enough to each other to form protein complexes. Indeed, endogenous YTHDF2 coimmunoprecipitated with FLAG-MAGEL2 produced in tetracycline-induced stable HEK293-MAGEL2 cells (Fig. 6*B*). As a control, endogenous USP7 also coimmunoprecipitated with MAGEL2 (Fig. 6*B*) (8). Transient transfection and immunoprecipitation of FLAG-tagged YTHDF1, YTHDF2, or YTHDF3 coimmunoprecipitated coexpressed V5-MAGEL2, demonstrating that MAGEL2 and each of the three YTHDF proteins can form protein complexes, at least in this heterologous expression system (Fig. S8). However, recombinant V5-tagged CtermMAGEL2 did not coimmunoprecipitate with any of the YTHDF proteins, consistent with BioID results that showed YTHDF proteins in proximity to full-length MAGEL2 but not the C-terminal portion of MAGEL2. We also expected that MAGEL2 and YTHDF proteins should be present in the same cellular compartments. We transiently cotransfected U2OS cells, which have a larger cytoplasmic compartment than HEK293 cells so allow for improved visualization of recombinant proteins by confocal microscopy. MAGEL2 and each YTHDF protein are present diffusely in the cytoplasm, with signals overlapping in the cytoplasmic and perinuclear region of the cell (Fig. S9).

MAGEL2 has an expanded number of interactions after heat shock stress

YTHDF proteins are found in the cytosol and the nucleus, and all three YTHDF proteins partially relocalize to stress granules under stress conditions (117). To determine whether

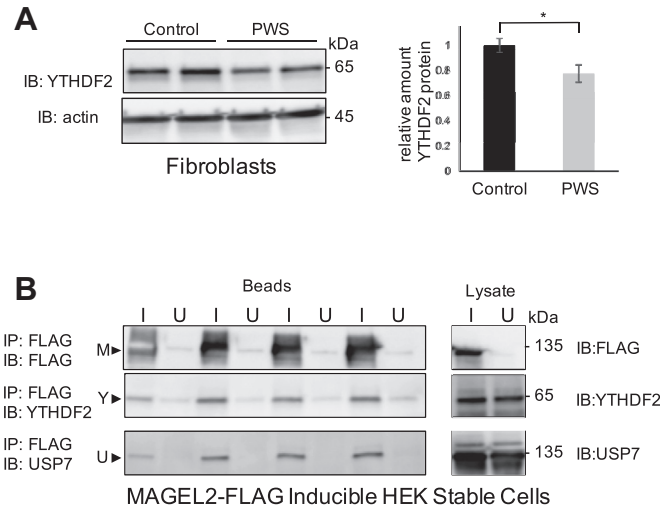

Figure 6. Human fibroblasts from individuals with PWS have less YTHDF2 protein than control fibroblasts, and endogenous USP7 and YTHDF2 proteins coimmunoprecipitate with MAGEL2. *A*, endogenous YTHDF2 protein levels were measured by immunoblotting lysates from cultured immortalized fibroblasts. C12 and C14 are fibroblast lines from control individuals, whereas P16 and P21 are fibroblast cell lines from individuals with PWS lacking MAGEL2 expression. *Right*, analysis of replicate blots of YTHDF2 levels in control and PWS fibroblasts, with equal amounts of total protein loaded per lane (mean ± standard error of the mean, n = 8 per genotype, **p* = 0.03 by Student *t* test). *B*, quadruplicate samples of MAGEL2-HEK cells were induced (I) or uninduced (U) to express full-length MAGEL2 (M). Endogenous YTHDF2 and endogenous USP7 coimmunoprecipitated with FLAG-MAGEL2 using anti-FLAG M2 gel. 10% of each cell lysate was immunoblotted to confirm the presence of all proteins in the input lysates.

MAGEL2 protein–protein interactions are sensitive to stress, we induced MAGEL2 expression in HEK293-MAGEL2 cells, treated with biotin, heat shocked the cells at 42 °C for 1 h, then processed the cell lysates for BioID-MS. After eliminating proteins found in only one of three replicate samples or present at high levels the CRAPome, 364 MAGEL2-proximal proteins were identified in heat-shocked HEK293-MAGEL2 cells, including 33 of the 34 MAGEL2 proximal proteins identified under nonstressed conditions (Table S2). The heat-shocked MAGEL2 proximity interactome was enriched for ribosomal proteins and RNA-binding processes such as mRNA metabolism and mRNA splicing. In a parallel experiment, 768 proximal proteins enriched for ribosomal proteins and proteins involved in mRNA metabolism and translation initiation were in proximity to CtermMAGEL2 after heat shock (Table S2).

We next asked whether coexpression of MAGEL2 might modify the responses of YTHDF2 to heat shock. YTHDF2, an m^6A "reader," regulates 5′UTR methylation and translation initiation under conditions of stress, in part by relocalizing to the nucleus to prevent demethylation by m^6A "erasers" (118). Expression of MAGEL2 was induced (or not) in HEK293-MAGEL2 cells, then cells were heat shocked in a 42 °C water bath for 1 h and harvested at time intervals thereafter. Cells were fractionated into nuclear and cytoplasmic fractions, in three replicate trials (119) (Fig. 7*A*). The amount of nuclear YTHDF2 protein under each condition was normalized to the whole cell protein and plotted over time (Fig. 7*B*). In response to heat shock, the proportion of YTHDF2 found in the nuclear fraction after heat shock increased in uninduced HEK293-MAGEL2 cells, compared with before heat shock (repeated measures ANOVA, F = 7.7 F crit = 4.4, n = 3, p = 0.01). However, induction of MAGEL2 expression in HEK293-MAGEL2 prevented the redistribution of YTHDF2 protein into the nucleus after heat shock ($p > 0.05$).

Discussion

MAGEL2 is mutated in people with SYS and inactivated in people with PWS, but how the loss of MAGEL2 function contributes to pathophysiology these disorders is unknown. Identifying the proteins proximal to MAGEL2 could shed light into the function of this enigmatic protein, and particularly the function of the N-terminal region of MAGEL2 that has not previously been studied. Our bioinformatic analysis revealed that the N-terminal portion of MAGEL2 contains intrinsically disordered protein domains with a highly predicted propensity toward protein phase separation. We used proximity-based biotinylation (BioID) coupled with mass spectrometry to identify MAGEL2-proximal proteins, many of which were previously shown to physically associate with each other. The C-terminal proximal proteins formed clusters of interacting proteins that function in RNA metabolic processes, stress response, and metabolism. Proximal proteins were enriched for GO terms such as cadherin binding, ribonucleoprotein complex binding, translation initiation, and RNA binding and processing. When merged with processes ascribed to previously identified MAGEL2-interacting proteins, such as Arp2/3 complex-mediated actin nucleation, ubiquitination, and retrograde transport, our study points to possible novel roles for CtermMAGEL2.

The proteins proximal to CtermMAGEL2 differed when structure-altering mutations were made in the C-terminal MAGE homology domain. For example, the coding region instability determinant binding proteins YBX1 and DHX9 were proximal to wild-type MAGEL2, but were not proximal to the MHD-mutated MAGEL2 proteins. We recently demonstrated that analogous mutations in the MHD of necdin, another MAGE protein, alter the necdin protein interactome (88). Interestingly, MAGE proteins carrying an arginine to cysteine MHD mutation, that is, MAGEL2p.R1187C and NDNp.R265C modeled on the Bartter syndrome mutation MAGED2p.R446C, had more BioID-identified proximal proteins than wild-type ((88) and this report). In contrast, both CtermMAGEL2p.LL1031AA (this study) and NDNp.VL109AA (88) had fewer proximal proteins than their wild-type counterparts. These changes in interaction could be physiologically relevant, given that pathogenic mutations in the MHD of MAGEG1/NSMCE3 cause a chromosome breakage syndrome by disrupting interactions with NSCME4, thus destabilizing the SMC5/6 complex (17, 120). BioID-MS could be a valuable tool for the evaluation of coding variants of unknown significance in *MAGEL2* or other MAGE genes associated with disease (16–24).

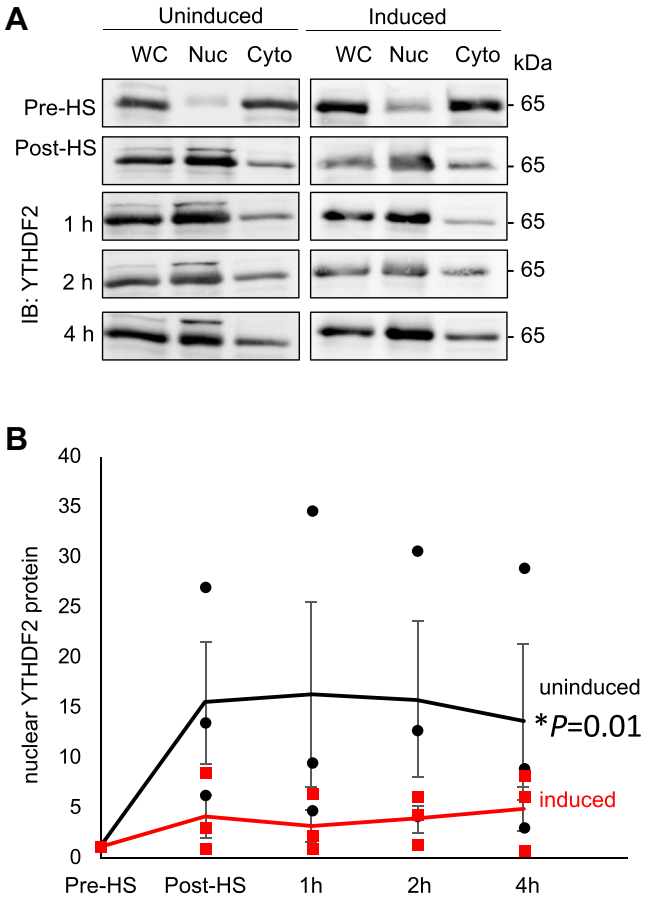

Figure 7. YTHDF2 protein levels in the nucleus change in response to heat shock, and MAGEL2 expression blunts this response. *A*, HEK293-MAGEL2 cells that were either induced with tetracycline to express MAGEL2, or uninduced, were placed in a 42 °C water bath for 1 h. Cells were harvested at different time points, before heat shock (Pre-HS), immediately following heat shock (Post-HS) or at 1, 2, and 4 h following removal of the samples from the water bath. Proteins from cellular fractions (whole cell, WC, or nuclear fraction, Nuc, or cytoplasmic fraction, Cyto) were immunoblotted to examine the abundance of endogenous YTHDF2. Equal amounts of protein were loaded. A representative trial is shown. *B*, the change in the proportion of YTHDF2 in the nucleus relative to preheat shock in induced (MAGEL2-expressing) and uninduced cells was plotted over time for triplicate samples, normalized to the amount of YTHDF2 in the nuclear fraction a pre-heat shock (uninduced, *black* and induced, *red*, mean ± standard deviation, individual triplicate values are also shown). The relative amount of YTHDF2 protein in the nucleus increases after heat shock in uninduced (*black*, no MAGEL2 expression) HEK293-MAGEL2 cells (repeated measures ANOVA, $*p < 0.01$, n = 3). There was no change in relative levels of nuclear endogenous YTHDF2 levels after heat shock in induced, MAGEL2-expressing cells (*red circles*, repeated measures ANOVA, $*p > 0.05$, n = 3).

The most novel part of our study is the analysis of proteins proximal to the N-terminal region of MAGEL2. Proteins with high phase separation prediction values are preferentially associated with GO terms such as phase-separated compartments (*e.g.*, stress granules and postsynaptic densities), in RNA processing, in the assembly and plasticity of structural components, and in signaling, regulation, and development (64). MAGEL2-proximal proteins are highly associated with an overlapping set of GO terms, in particular RNA processing activities, consistent with the high phase separation prediction score that we identified for the N-terminal region of MAGEL2. Two sets of RNA-binding proteins, TNRC6A and TNRC6B (trinucleotide repeat containing adaptor 6 A/B), and YTHDF1, YTHDF2, and YTHDF3 (YTH N^6-methyladenosine RNA-binding protein 1/2/3), were proximal to full-length MAGEL2 but not to C-terminal MAGEL2. TNRC6A and TNRC6B are paralogs of the *Drosophila* GW182 scaffolding proteins and act in posttranscriptional gene silencing through RNAi and microRNA pathways. TNRC6A/B complexes with mRNAs and Argonaute proteins in P-bodies in the cytoplasm and can recruit CCR4-NOT and PAN deadenylase complexes to repress mRNAs (113).

Complexes containing YTHDF proteins and m^6A-modified mRNA partition into cellular phase-separated compartments that differentially regulate the stability and translation of the mRNAs (104, 117). YTHDF proteins have a conserved interaction domain in their C-terminal portion, namely the YTH domain that binds polymethylated m^6A modified mRNAs. They also have a low-complexity prion-like domain that contains P-X_n-G motifs, in their N-terminus (103, 117, 121). Like other low-complexity proteins, YTHDF proteins interact with each other and undergo warming-induced liquid–liquid phase separation, which allows them to form membraneless biomolecular condensates such as stress granules and processing bodies (P-bodies) (62, 122, 123). YTHDF2 regulates 5′UTR methylation and translation initiation under conditions of stress, in part by relocalizing to the nucleus to prevent demethylation by m^6A "erasers" (84, 118, 121). We show that MAGEL2 interacts with YTHDF2 by BioID and coimmunoprecipitation. In addition, we found that in response to heat stress, YTHDF2 moves to the nucleus. However, MAGEL2 expression abrogated the increase of YTHDF2 in the nucleus after heat shock. These data suggest that MAGEL2 could regulate the translocation of YTHDF2 to the nucleus, by an as yet unknown mechanism (124).

Like YTHDF proteins, MAGEL2 contains Pro-X_n-Gly motifs in its N-terminal region, which is predicted to be an intrinsically disordered domain. MAGEL2 is predicted to undergo phase separation and localize to membraneless compartments in the cell, perhaps accounting for the large number of proteins in proximity to MAGEL2 under conditions of stress. Interestingly, the N-terminal portion of MAGEL2 has more P-X_n-G motifs and a smaller spacing between them than the YTHDF proteins. In contrast elastin, a prototypical P-X_n-G intrinsically disordered self-assembling protein, has a denser arrangement of P-X_n-G motifs than the N-terminal domains of either MAGEL2 or YTHDF. The most common mutations in SYS cause a frameshift at glutamine at position 666, potentially resulting in the production of a truncated protein encoding only the Pro-X_n-Gly-rich, intrinsically disordered N-terminus of MAGEL2. A MAGEL2 truncated protein could impair the dynamics of ribonucleoprotein bodies that undergo liquid–liquid phase separation. This supports a model that SYS-causing frameshift mutations encode a truncated MAGEL2 protein that could be prone to pathological aggregation in RNA-rich granules when no longer associated with the structured C-terminus. There is no biological evidence that this occurs in individuals with SYS, in part because MAGEL2 is only expressed in discrete regions of the brain. However, we

did previously find changes in the abundance of p62-rich cytoplasmic inclusions in muscle and hypothalamus of mice carrying a mutation in the *Magel2* gene that results in a truncated Magel2 protein (5). A toxic aggregation model would also explain the more severe and sometimes fatal outcomes associated with MAGEL2 frameshift and stop mutations causing SYS, compared with the typical presentation in PWS, in which the MAGEL2 gene is inactivated completely and MAGEL2 protein is absent (24).

Notably, the missense mutations that we investigated were in the MAGE homology domain in the folded region of MAGEL2. Mutations in intrinsically disordered regions of proteins, such as the N-terminal region of MAGEL2, are more challenging to evaluate (61). Many autism spectrum disorder susceptibility genes encode proteins that function in RNA processing, activity-dependent translation, and synaptic function (125). Furthermore, both phase separation and the partitioning of proteins in the cell can be disrupted by pathogenic mutations in these susceptibility genes (61). Given that frameshift mutations in MAGEL2 cause autism spectrum disorder, our study raises the possibility that an untapped reservoir of mutations in the intrinsically disordered N-terminus of MAGEL2 could contribute to some of the missing heritability in neurodevelopmental disorders.

Our study has some limitations. BioID can detect weak, transient, or indirect protein–protein interactions, so the proteins identified as part of the MAGEL2 interactome may reside at a further distance from MAGEL2 than proteins identified as direct interactors by other methods. The HEK293-Flp-In cell line used for these experiments was ideal for comparison of BioID results for different MAGEL2 proteins because of the single integration site and ability to induce low level expression of MAGEL2, in contrast to overexpression systems. While HEK293 cells have some neuronal phenotypes (126), they do not normally express *MAGEL2*, so some proximal proteins may not be physiologically relevant in the tissues where MAGEL2 is normally expressed, such as the brain, muscle, and bone. The use of recombinant proteins and the location of the BirA* tag were also limitations of the study. MAGEL2 proteins carried N-terminal BirA* tags, which was ideal for comparison among the variant MAGEL2 proteins, but complementary studies using C-terminally tagged MAGEL2 proteins would be informative. To further expand our knowledge of the MAGEL2 interactome, we compared proteins proximal to the full-length MAGEL2 protein, which has not been studied previously, to proteins proximal to the C-terminal half of MAGEL2. The results suggest that the N- and C-terminal domains of MAGEL2 are both important for protein interactions. It is unclear why there are certain proteins proximal to CtermMAGEL2 and not the full-length protein. It is possible that without the N-terminal portion of the protein, the MHD is more available to bind proteins. Alternatively, the N-terminus could obscure proteins that complex with the C-terminus, or the unstructured nature of the N-terminus could increase the volume that the protein occupies, putting the C-terminus out of the 10 nm labeling range of the biotin ligase (127). Unfortunately, we were not able to express the N-terminal region of the protein alone, nor test whether presumptive N-terminal proximal proteins indeed interact with the N-terminus of the protein.

In conclusion, we used proximity-dependent labeling and mass spectrometry to identify novel proteins in proximity to MAGEL2. When we analyzed the proximal MAGEL2 and CtermMAGEL2 together using STRING, we found that they form a large network of proteins that function in translation initiation and ubiquitination. The 13 proteins that are proximal to both MAGEL2 and CtermMAGEL2 represent the proteins that are the highest confidence for being direct interactors of MAGEL2. The 22 proteins that interact with only the full-length protein represent novel subjects for the focus of MAGEL2 functional experiments, particularly in the area of RNA processing and phase separation. Further studies are needed to determine whether BioID-MS can be used to examine the functional impact of MAGEL2 missense mutations identified in individuals carrying a clinical diagnosis of SYS. The functional pathways identified among MAGEL2-proximal proteins indicate potential avenues of investigation to understand the cellular functions disrupted in both PWS and SYS.

Experimental procedures

Bioinformatic protein analysis

The NCBI Conserved Domain Database (CDD v.3.17) was used to analyze MAGEL2 protein (CCDS73700) for motifs (55). Protein Data Bank (128) Protein Feature View (https://www.rcsb.org) was used to visualize disordered *versus* ordered regions (computed by JRONN (129)) and hydropathy, calculated using a sliding window of 15 residues and summing up scores from standard hydrophobicity tables. Amino acid composition was visualized using PLAAC (Prion-like amino acid composition) (130). Predicted phase separation propensities (PScore) were calculated using Pscore Predictor (64). Probability scores for intrinsically disordered protein regions were calculated using SPOT-Disorder2, with a score >0.46 indicating an intrinsically disordered protein region (60). Identification of Pro-X_n-Gly motifs in proteins was performed in MATLB using Script 1 (62).

Plasmid construction

pENTR clones containing CtermMAGEL2p.LL1031AA and CtermMAGELp.R1187C were created in the wild-type pENTR-CtermMAGEL2cDNA (DNASU Clone: HsCD00295122, NCBI Reference Sequences: NM_019066.5 and NP_061939.3) by site-directed mutagenesis. Mutations in MAGEL2 were as follows: p.Leu1031_Leu1032delinsAlaAla (p.VL1031AA, c.[C1281CG;T1282C;C1284G;T1285C]), and p.Arg1187Cys (p.R1187C, c.[C1750T;A1752T]. In brief, tail-to-tail oligonucleotide primers containing the desired missense mutation were used for PCR amplification of pENTR-CtermMAGEL2. The PCR product was digested with DpnI, phosphorylated, and recircularized by ligation. The presence of the respective mutations was confirmed by sequencing. MAGEL2, CtermMAGEL2, and mutant

CtermMAGEL2 cDNAs were transferred to pDEST-pcDNA5-BirA*-FLAG using gateway recombinational cloning to create FLAG-BirA*-MAGEL2, FLAG-BirA*-CtermMAGEL2, and mutant FLAG-BirA*-CtermMAGEL2 constructs (7, 67). FLAG-YTHDF1, FLAG-YTHDF2, and FLAG-YTHDF3 were provided by Dr Chuan He (131). Plasmids pOG44 and pDEST-pcDNA5-BirA*-FLAG were provided by Dr A-C Gingras (67).

Cell culture, cell lines, and transfections

Tissue culture reagents were from Thermo-Fisher Scientific unless otherwise stated. Flp-In T-Rex HEK293 cells (Invitrogen) were cultured in Dulbecco's modified Eagle medium (DMEM) supplemented with 10% fetal bovine serum, 1% L-glutamine, and 1% penicillin/streptomycin at 37 °C with 5% CO_2, and maintained in zeocin (100 μg/ml) and blasticidin (15 μg/ml) (132, 133). To generate stable cell lines, Flp-In T-Rex HEK293 cells were seeded at a density of 1×10^5 cells per well in a 6-well plate and cotransfected 24 h later with pOG44 and pcDNA FLAG-BirA* constructs at a ratio of 9:1 using FuGENE6 (Promega E2691). Cells were then cultured in media without zeocin or blasticidin, but with hygromycin B (100 μg/ml) to select for cells carrying stable integration of the construct. These cell lines, carrying FLAG-BirA*-MAGEL2 constructs, are called HEK293-MAGEL2, HEK293-CtermMAGEL2, or HEK293-mutantCtermMAGEL2. For heat shock experiments, HEK293-MAGEL2 cells that had or had not been induced for MAGEL2 expression were placed in a 42 °C water bath for 1 h. Lysates were harvested at different time points, before heat shock, immediately following heat shock, and then at 1 h, 2 h, and 4 h following removal from the water bath. Cellular fractionation was performed on the lysates using the REAP 2 min nonionic detergent-based purification technique (119). Human control fibroblasts (FB12 NIGMS repository number GM01601A, FB14 GM00650) were from the NIGMS human genetic cell repository (Camden NJ). PWS fibroblasts (15q11-q13 deletion) were FB16 (1889 PWS) from the Brain and Tissue Banks for Developmental Disorders, and PWS129 from Dr Daniel Driscoll University of Florida Gainesville, and RCB1560 from RIKEN Bioresource Centre Cell Bank in Tsukuba Japan. Cell lines are regularly tested for *mycoplasma*.

Proximity-dependent biotin identification coupled to affinity capture and mass spectrometry

Stably transfected HEK293-MAGEL2, HEK293-CtermMAGEL2, or HEK293-mutantCtermMAGEL2 cells were cultured in 10 cm dishes and incubated overnight with 1 μg/ml tetracycline and 50 μM biotin. Cells were washed twice with 10 ml PBS to remove excess biotin prior to collection. BioID analysis was adapted from previously described methods (7, 68), with the following modifications: cells were lysed in 2.2 ml of lysis buffer (50 mM Tris HCl, 500 mM NaCl, 0.2% SDS, 2% Triton-X, pH 8.0, 1× Complete Mini Protease Inhibitor (Roche)), 150 μl of streptavidin sepharose beads were used in the affinity capture, and the beads were washed four times with 100 mM ammonium bicarbonate (AmBic), then reduced (10 mM beta-mercaptoethanol in 100 mM AmBic) and alkylated (55 mM iodoacetamide in 100 mM AmBic). Trypsin (150 μl of 6 ng/μl, Promega Sequencing grade, specifically cleaves at the carboxylic side of lysine and arginine residues) was added, and the digestion was allowed to proceed overnight (~16 h) at 30 °C. The supernatant was collected and the beads were washed with 100 μl of extraction buffer (97% water/2% acetonitrile/1% formic acid) followed by a second 100 μl wash with 50% extraction buffer and 50% acetonitrile. Both washes were combined with the initial supernatant, and the samples were then dried under vacuum and then dissolved in 80 μl 0.3% formic acid.

Samples were resolved and ionized by using nanoflow HPLC (Easy-nLC II, Thermo Scientific) with a PicoFrit fused silica capillary column (ProteoPepII, C18) with 100 μm inner diameter (300 Å, 5 μm, New Objective) coupled to an LTQ XL-Orbitrap hybrid mass spectrometer (Thermo Scientific). Peptide mixtures were injected (10 μl) onto the column and resolved at 500 nl/min using a 60 min linear gradient from 0 to 35% v/v aqueous ACN in 0.2% v/v formic acid. The mass spectrometer was operated in data-dependent acquisition mode, recording high-accuracy and high-resolution survey Orbitrap spectra using external mass calibration, with a resolution of 30,000 and m/z range of 400 to 2000. The 14 most intense multiply charged ions were sequentially fragmented by using collision induced dissociation. Data was processed using Proteome Discoverer 1.4 (Thermo Scientific) and a human proteome database (UniProtUP000005640, version 2016_10, *Homo sapiens*, 70,671 entries) was searched using SEQUEST (Thermo Scientific). Search parameters included a precursor mass tolerance of 10 ppm and a fragment mass tolerance of 0.8 Da. Peptides were searched with carbamidomethyl cysteine as a static modification and oxidized methionine and deamidated glutamine and asparagine as dynamic modifications.

Mass spectrometry data processing and bioinformatics

Two missed cleavages were permitted. The XCorr threshold value was 0.4, and the fragment ion cutoff percentage was 0.1. False discovery rate (FDR) calculations were not needed for these small datasets. There were no single peptide identifications of proteins. All original mass spectrometry data, including the number of distinct peptides assigned for each protein and the % coverage of each protein assigned, is included in Table S2. Individual replicate reports for each stable cell line were compiled into a multiconsensus report to facilitate comparisons among replicate samples. Commonly identified contaminating proteins (keratins, acetyl-CoA carboxylase alpha, acetyl-CoA carboxylase beta, pyruvate carboxylase, propionyl-CoA carboxylase, and methylcrotonyl-CoA carboxylase 1) were systematically removed. We then consulted lists of proteins identified in similar BioID studies (CRAPome (70)) and removed proteins from the reports that fit the following parameters: epitope tag BirA*-FLAG, cell type HEK293, and affinity approach streptavidin, score of 50 or greater. Known and predicted protein–protein interactions

were analyzed using STRING version 10.5 (string-db.org) and refined with literature searches. Interactions that were based on experiments rather than on text-mining or coexpression were included, and the minimum required interaction score was set to the default value (medium confidence, 0.4). MAGEL2-proximal proteins were analyzed using the Cytoscape app ClueGO to reveal functional enrichment of GO terms. The analyses included GO Biological Process, GO Molecular Function, and REACTOME Pathways.

Immunoblotting and immunofluorescence

Immunoblots were performed as previously described (15). Primary antibodies included rabbit anti-FLAG (Sigma F7425 1:15,000), mouse anti-V5 (Abcam #ab27671, 1:5000), rabbit anti-YTHDF2 (Proteintech #24744-1AP, 1:5000), rabbit anti-USP7 (Abcam ab4080, 1:1000), and HRP-conjugated anti-actin (Sigma #A3854, 1:10,000). Secondary antibodies included HRP-linked donkey anti-rabbit IgG (Amersham Pharmacia Biotech #NA934, 1:5000) and HRP-linked sheep anti-mouse (Amersham Pharmacia Biotech #RPN4201, 1:5000). For immunofluorescence microscopy, stably transfected HEK293-MAGEL2 cells were plated onto coverslips precoated with poly-L lysine, induced in tetracycline (1 μg/ml) for 24 h, and then processed as described (15) using rabbit anti-FLAG (Sigma F7425 1:1000) or mouse anti-V5 (Abcam #ab27671, 1:1000) and Alexa Fluor 488 or 594-linked goat anti-rabbit secondary antibody (Thermofisher Scientific #A-11034 or #A-11012, 1:1000) or Alexa Fluor 488- or 594-linked goat anti-mouse (Thermofisher Scientific #A-11001 or #A-11005, 1:1000) then imaged using a Zeiss LSM 700 confocal microscope with a 40x or 63x oil immersion lens (N. A. 1.4 oil). Coimmunoprecipitation for the MAGEL2 interactors YTHDF1/2/3 was performed as previously described (134). After retaining 10% of the cell lysate as input, lysates were precleared with 20 μl Sepharose 4B beads (Sigma) for 1 h at 4 °C on a rocker. Lysates were then probed with anti-FLAG M2 affinity gel (Sigma) and mixed end-over-end at 4 °C for 2 h. Beads were washed three times (50 mM Tris-Cl pH 8.0, 150 mM NaCl, and 0.5% IGEPAL) and resuspended in 50 μl 2× Laemmli buffer (62.5 mM Tris-HCl, 3% SDS, 10% glycerol), 2% beta-mercaptoethanol, and 1% bromophenol blue. Bound proteins were eluted from beads by boiling for 10 min. Immunoblots of input samples and immunoprecipitates were performed as described above.

Statistics for replicate stability bioassays

Continuous data are presented as mean ± SD of 3 to 4 replicates per experiment. Differences between means were evaluated using a Student's t test and considered significant if $p < 0.05$. Group differences using two factors were evaluated by two-way ANOVA to determine if there was an effect of MAGEL2 expression and heat stress on the amount of YTHDF2 protein in the nucleus. Results were considered significant if $p < 0.05$.

Data availability

Data are available on MassIVE (Mass Spectrometry Interactive Virtual Environment, ftp://massive.ucsd.edu/MSV000087525).

Supporting information—This article contains supporting information.

Acknowledgments—We thank Jack Moore and the Alberta Proteomics and Mass Spectrometry Facility, Adam Casey for assistance with MATLB scripts and Jocelyn Bischof for technical assistance. We gratefully acknowledge operating funding from the Foundation for Prader–Willi Research.

Author contributions—M. R. S. and R. W. conceptualization; M. R. S. and R. W. formal analysis; R. W. funding acquisition; M. R. S. investigation; M. R. S., R. P. F., and R. W. methodology; R. W. project administration; R. P. F. and R. W. resources; R. W. supervision; M. R. S. validation; M. R. S. writing—original draft; M. R. S., R. P. F., and R. W. writing—review and editing.

Conflicts of interest—The authors declare that they have no conflicts of interest with the contents of this article.

Abbreviations—The abbreviations used are: BioID, proximity-dependent biotin identification; CRAPome, contaminant repository for affinity purification–mass spectrometry data; MAGE, melanoma-associated antigen gene; MHD, MAGE homology domain; LC-MS/MS, Liquid chromatography–tandem mass spectrometry; PWS, Prader–Willi syndrome; SYS, Schaaf–Yang syndrome.

References

1. Weon, J. L., and Potts, P. R. (2015) The MAGE protein family and cancer. *Curr. Opin. Cell Biol.* **37**, 1–8
2. Lee, A. K., and Potts, P. R. (2017) A comprehensive guide to the MAGE family of ubiquitin ligases. *J. Mol. Biol.* **429**, 1114–1142
3. Feng, Y., Gao, J., and Yang, M. (2011) When MAGE meets RING: Insights into biological functions of MAGE proteins. *Protein Cell* **2**, 7–12
4. Doyle, J. M., Gao, J., Wang, J., Yang, M., and Potts, P. R. (2010) MAGE-RING protein complexes comprise a family of E3 ubiquitin ligases. *Mol. Cell* **39**, 963–974
5. Kamaludin, A. A., Smolarchuk, C., Bischof, J. M., Eggert, R., Greer, J. J., Ren, J., Lee, J. J., Yokota, T., Berry, F. B., and Wevrick, R. (2016) Muscle dysfunction caused by loss of Magel2 in a mouse model of Prader-Willi and Schaaf-Yang syndromes. *Hum. Mol. Genet.* **25**, 3798–3809
6. Hao, Y. H., Doyle, J. M., Ramanathan, S., Gomez, T. S., Jia, D., Xu, M., Chen, Z. J., Billadeau, D. D., Rosen, M. K., and Potts, P. R. (2013) Regulation of WASH-dependent actin polymerization and protein trafficking by ubiquitination. *Cell* **152**, 1051–1064
7. Wijesuriya, T. M., De Ceuninck, L., Masschaele, D., Sanderson, M. R., Carias, K. V., Tavernier, J., and Wevrick, R. (2017) The Prader-Willi syndrome proteins MAGEL2 and necdin regulate leptin receptor cell surface abundance through ubiquitination pathways. *Hum. Mol. Genet.* **26**, 4215–4230
8. Hao, Y. H., Fountain, M. D., Jr., Fon Tacer, K., Xia, F., Bi, W., Kang, S. H., Patel, A., Rosenfeld, J. A., Le Caignec, C., Isidor, B., Krantz, I. D., Noon, S. E., Pfotenhauer, J. P., Morgan, T. M., Moran, R., *et al.* (2015) USP7 acts as a molecular rheostat to promote WASH-dependent endosomal protein recycling and is mutated in a human neurodevelopmental disorder. *Mol. Cell* **59**, 956–969
9. Carias, K. V., Zoeteman, M., Seewald, A., Sanderson, M. R., Bischof, J. M., and Wevrick, R. (2020) A MAGEL2-deubiquitinase complex

modulates the ubiquitination of circadian rhythm protein CRY1. *PLoS One* **15**, e0230874
10. Crutcher, E., Pal, R., Naini, F., Zhang, P., Laugsch, M., Kim, J., Bajic, A., and Schaaf, C. P. (2019) mTOR and autophagy pathways are dysregulated in murine and human models of Schaaf-Yang syndrome. *Sci. Rep.* **9**, 15935
11. Boccaccio, I., Glatt-Deeley, H., Watrin, F., Roeckel, N., Lalande, M., and Muscatelli, F. (1999) The human MAGEL2 gene and its mouse homologue are paternally expressed and mapped to the Prader-Willi region. *Hum. Mol. Genet.* **8**, 2497–2505
12. Devos, J., Weselake, S. V., and Wevrick, R. (2011) Magel2, a Prader-Willi syndrome candidate gene, modulates the activities of circadian rhythm proteins in cultured cells. *J. Circadian Rhythms* **9**, 12
13. Gur, I., Fujiwara, K., Hasegawa, K., and Yoshikawa, K. (2014) Necdin promotes ubiquitin-dependent degradation of PIAS1 SUMO E3 ligase. *PLoS One* **9**, e99503
14. Kuwako, K., Taniura, H., and Yoshikawa, K. (2004) Necdin-related MAGE proteins differentially interact with the E2F1 transcription factor and the p75 neurotrophin receptor. *J. Biol. Chem.* **279**, 1703–1712
15. Lee, S., Walker, C. L., Karten, B., Kuny, S. L., Tennese, A. A., O'Neill, M. A., and Wevrick, R. (2005) Essential role for the Prader-Willi syndrome protein necdin in axonal outgrowth. *Hum. Mol. Genet.* **14**, 627–637
16. Laghmani, K., Beck, B. B., Yang, S. S., Seaayfan, E., Wenzel, A., Reusch, B., Vitzthum, H., Priem, D., Demaretz, S., Bergmann, K., Duin, L. K., Gobel, H., Mache, C., Thiele, H., Bartram, M. P., *et al.* (2016) Polyhydramnios, transient Antenatal Bartter's syndrome, and MAGED2 mutations. *N. Engl. J. Med.* **374**, 1853–1863
17. van der Crabben, S. N., Hennus, M. P., McGregor, G. A., Ritter, D. I., Nagamani, S. C., Wells, O. S., Harakalova, M., Chinn, I. K., Alt, A., Vondrova, L., Hochstenbach, R., van Montfrans, J. M., Terheggen-Lagro, S. W., van Lieshout, S., van Roosmalen, M. J., *et al.* (2016) Destabilized SMC5/6 complex leads to chromosome breakage syndrome with severe lung disease. *J. Clin. Invest.* **126**, 2881–2892
18. Tacer, K. F., and Potts, P. R. (2017) Cellular and disease functions of the Prader-Willi syndrome gene MAGEL2. *Biochem. J.* **474**, 2177–2190
19. Okutman, O., Muller, J., Skory, V., Garnier, J. M., Gaucherot, A., Baert, Y., Lamour, V., Serdarogullari, M., Gultomruk, M., Ropke, A., Kliesch, S., Herbepin, V., Aknin, I., Benkhalifa, M., Teletin, M., *et al.* (2017) A no-stop mutation in MAGEB4 is a possible cause of rare X-linked azoospermia and oligozoospermia in a consanguineous Turkish family. *J. Assist. Reprod. Genet.* **34**, 683–694
20. Lo Giacco, D., Chianese, C., Ars, E., Ruiz-Castane, E., Forti, G., and Krausz, C. (2014) Recurrent X chromosome-linked deletions: Discovery of new genetic factors in male infertility. *J. Med. Genet.* **51**, 340–344
21. Tsang, Y. H., Wang, Y., Kong, K., Grzeskowiak, C., Zagorodna, O., Dogruluk, T., Lu, H., Villafane, N., Bhavana, V. H., Moreno, D., Elsea, S. H., Liang, H., Mills, G. B., and Scott, K. L. (2020) Differential expression of MAGEA6 toggles autophagy to promote pancreatic cancer progression. *Elife* **9**, e48963
22. Pineda, C. T., and Potts, P. R. (2015) Oncogenic MAGEA-TRIM28 ubiquitin ligase downregulates autophagy by ubiquitinating and degrading AMPK in cancer. *Autophagy* **11**, 844–846
23. Schaaf, C. P., Gonzalez-Garay, M. L., Xia, F., Potocki, L., Gripp, K. W., Zhang, B., Peters, B. A., McElwain, M. A., Drmanac, R., Beaudet, A. L., Caskey, C. T., and Yang, Y. (2013) Truncating mutations of MAGEL2 cause Prader-Willi phenotypes and autism. *Nat. Genet.* **45**, 1405–1408
24. Fountain, M. D., and Schaaf, C. P. (2016) Prader-Willi syndrome and Schaaf-Yang syndrome: Neurodevelopmental diseases intersecting at the MAGEL2 gene. *Diseases* **4**, 2
25. Chen, H., Victor, A. K., Klein, J., Tacer, K. F., Tai, D. J., de Esch, C., Nuttle, A., Temirov, J., Burnett, L. C., Rosenbaum, M., Zhang, Y., Ding, L., Moresco, J. J., Diedrich, J. K., Yates, J. R., 3rd, *et al.* (2020) Loss of MAGEL2 in Prader-Willi syndrome leads to decreased secretory granule and neuropeptide production. *JCI Insight* **5**, e138576
26. Xiao, B., Ji, X., Wei, W., Hui, Y., and Sun, Y. (2020) A recurrent variant in MAGEL2 in five siblings with severe respiratory disturbance after birth. *Mol. Syndromol.* **10**, 286–290
27. Fountain, M. D., Aten, E., Cho, M. T., Juusola, J., Walkiewicz, M. A., Ray, J. W., Xia, F., Yang, Y., Graham, B. H., Bacino, C. A., Potocki, L., van Haeringen, A., Ruivenkamp, C. A., Mancias, P., Northrup, H., *et al.* (2017) The phenotypic spectrum of Schaaf-Yang syndrome: 18 new affected individuals from 14 families. *Genet. Med.* **19**, 45–52
28. McCarthy, J., Lupo, P. J., Kovar, E., Rech, M., Bostwick, B., Scott, D., Kraft, K., Roscioli, T., Charrow, J., Schrier Vergano, S. A., Lose, E., Smiegel, R., Lacassie, Y., and Schaaf, C. P. (2018) Schaaf-Yang syndrome overview: Report of 78 individuals. *Am. J. Med. Genet. A* **176**, 2564–2574
29. Guo, W., Nie, Y., Yan, Z., Zhu, X., Wang, Y., Guan, S., Kuo, Y., Zhang, W., Zhi, X., Wei, Y., Yan, L., and Qiao, J. (2019) Genetic testing and PGD for unexplained recurrent fetal malformations with MAGEL2 gene mutation. *Sci. China Life Sci.* **62**, 886–894
30. Enya, T., Okamoto, N., Iba, Y., Miyazawa, T., Okada, M., Ida, S., Naruto, T., Imoto, I., Fujita, A., Miyake, N., Matsumoto, N., Sugimoto, K., and Takemura, T. (2018) Three patients with Schaaf-Yang syndrome exhibiting arthrogryposis and endocrinological abnormalities. *Am. J. Med. Genet. A* **176**, 707–711
31. Jobling, R., Stavropoulos, D. J., Marshall, C. R., Cytrynbaum, C., Axford, M. M., Londero, V., Moalem, S., Orr, J., Rossignol, F., Lopes, F. D., Gauthier, J., Alos, N., Rupps, R., McKinnon, M., Adam, S., *et al.* (2018) Chitayat-Hall and Schaaf-Yang syndromes:a common aetiology: Expanding the phenotype of MAGEL2-related disorders. *J. Med. Genet.* **55**, 316–321
32. Buers, I., Persico, I., Schoning, L., Nitschke, Y., Di Rocco, M., Loi, A., Sahi, P. K., Utine, G. E., Bayraktar-Tanyeri, B., Zampino, G., Crisponi, G., Rutsch, F., and Crisponi, L. (2020) Crisponi/cold-induced sweating syndrome: Differential diagnosis, pathogenesis and treatment concepts. *Clin. Genet.* **97**, 209–221
33. Kleinendorst, L., Pi Castan, G., Caro-Llopis, A., Boon, E. M. J., and van Haelst, M. M. (2018) The role of obesity in the fatal outcome of Schaaf-Yang syndrome: Early onset morbid obesity in a patient with a MAGEL2 mutation. *Am. J. Med. Genet. A* **176**, 2456–2459
34. Urreizti, R., Cueto-Gonzalez, A. M., Franco-Valls, H., Mort-Farre, S., Roca-Ayats, N., Ponomarenko, J., Cozzuto, L., Company, C., Bosio, M., Ossowski, S., Montfort, M., Hecht, J., Tizzano, E. F., Cormand, B., Vilageliu, L., *et al.* (2017) A de novo nonsense mutation in MAGEL2 in a patient initially diagnosed as Opitz-C: Similarities between Schaaf-Yang and Opitz-C syndromes. *Sci. Rep.* **7**, 44138
35. Bayat, A., Bayat, M., Lozoya, R., and Schaaf, C. P. (2018) Chronic intestinal pseudo-obstruction syndrome and gastrointestinal malrotation in an infantwith schaaf-yang syndrome - expanding the phenotypic spectrum. *Eur. J. Med. Genet.* **61**, 627–630
36. Matuszewska, K. E., Badura-Stronka, M., Smigiel, R., Cabala, M., Biernacka, A., Kosinska, J., Rydzanicz, M., Winczewska-Wiktor, A., Sasiadek, M., Latos-Bielenska, A., Zemojtel, T., and Ploski, R. (2018) Phenotype of two Polish patients with Schaaf-Yang syndrome confirmed by identifying mutation in MAGEL2 gene. *Clin. Dysmorphol.* **27**, 49–52
37. Mejlachowicz, D., Nolent, F., Maluenda, J., Ranjatoelina-Randrianaivo, H., Giuliano, F., Gut, I., Sternberg, D., Laquerriere, A., and Melki, J. (2015) Truncating mutations of MAGEL2, a gene within the Prader-Willi locus, are responsible for severe arthrogryposis. *Am. J. Hum. Genet.* **97**, 616–620
38. Soden, S. E., Saunders, C. J., Willig, L. K., Farrow, E. G., Smith, L. D., Petrikin, J. E., LePichon, J. B., Miller, N. A., Thiffault, I., Dinwiddie, D. L., Twist, G., Noll, A., Heese, B. A., Zellmer, L., Atherton, A. M., *et al.* (2014) Effectiveness of exome and genome sequencing guided by acuity of illness for diagnosis of neurodevelopmental disorders. *Sci. Transl. Med.* **6**, 265ra168
39. Tong, W., Wang, Y., Lu, Y., Ye, T., Song, C., Xu, Y., Li, M., Ding, J., Duan, Y., Zhang, L., Gu, W., Zhao, X., Yang, X. A., and Jin, D. (2018) Whole-exome sequencing helps the diagnosis and treatment in children with neurodevelopmental delay accompanied unexplained dyspnea. *Sci. Rep.* **8**, 5214
40. Bischof, J. M., Stewart, C. L., and Wevrick, R. (2007) Inactivation of the mouse Magel2 gene results in growth abnormalities similar to Prader-Willi syndrome. *Hum. Mol. Genet.* **16**, 2713–2719

41. Baraghithy, S., Smoum, R., Drori, A., Hadar, R., Gammal, A., Hirsch, S., Attar-Namdar, M., Nemirovski, A., Gabet, Y., Langer, Y., Pollak, Y., Schaaf, C. P., Rech, M. E., Gross-Tsur, V., Bab, I., *et al.* (2019) Magel2 modulates bone remodeling and mass in Prader-Willi syndrome by affecting oleoyl serine levels and activity. *J. Bone Miner. Res.* **34**, 93–105
42. Fountain, M. D., Tao, H., Chen, C. A., Yin, J., and Schaaf, C. P. (2017) Magel2 knockout mice manifest altered social phenotypes and a deficit in preference for social novelty. *Genes Brain Behav.* **16**, 592–600
43. Kozlov, S. V., Bogenpohl, J. W., Howell, M. P., Wevrick, R., Panda, S., Hogenesch, J. B., Muglia, L. J., Van Gelder, R. N., Herzog, E. D., and Stewart, C. L. (2007) The imprinted gene Magel2 regulates normal circadian output. *Nat. Genet.* **39**, 1266–1272
44. Mercer, R. E., Kwolek, E. M., Bischof, J. M., van Eede, M., Henkelman, R. M., and Wevrick, R. (2009) Regionally reduced brain volume, altered serotonin neurochemistry, and abnormal behavior in mice null for the circadian rhythm output gene Magel2. *Am. J. Med. Genet. B Neuropsychiatr. Genet.* **150B**, 1085–1099
45. Luck, C., Vitaterna, M. H., and Wevrick, R. (2016) Dopamine pathway imbalance in mice lacking Magel2, a Prader-Willi syndrome candidate gene. *Behav. Neurosci.* **130**, 448–459
46. Oncul, M., Dilsiz, P., Ates Oz, E., Ates, T., Aklan, I., Celik, E., Sayar Atasoy, N., and Atasoy, D. (2018) Impaired melanocortin pathway function in Prader-Willi syndrome gene-Magel2 deficient mice. *Hum. Mol. Genet.* **27**, 3129–3136
47. Pravdivyi, I., Ballanyi, K., Colmers, W. F., and Wevrick, R. (2015) Progressive postnatal decline in leptin sensitivity of arcuate hypothalamic neurons in the Magel2-null mouse model of Prader-Willi syndrome. *Hum. Mol. Genet.* **24**, 4276–4283
48. Tennese, A. A., and Wevrick, R. (2011) Impaired hypothalamic regulation of endocrine function and delayed counterregulatory response to hypoglycemia in Magel2-null mice. *Endocrinology* **152**, 967–978
49. Mercer, R. E., and Wevrick, R. (2009) Loss of Magel2, a candidate gene for features of Prader-Willi syndrome, impairs reproductive function in mice. *PLoS One* **4**, e4291
50. Meziane, H., Schaller, F., Bauer, S., Villard, C., Matarazzo, V., Riet, F., Guillon, G., Lafitte, D., Desarmenien, M. G., Tauber, M., and Muscatelli, F. (2015) An early postnatal oxytocin treatment prevents social and learning deficits in adult mice deficient for Magel2, a gene involved in Prader-Willi syndrome and autism. *Biol. Psychiatry* **78**, 85–94
51. Schaller, F., Watrin, F., Sturny, R., Massacrier, A., Szepetowski, P., and Muscatelli, F. (2010) A single postnatal injection of oxytocin rescues the lethal feeding behaviour in mouse newborns deficient for the imprinted Magel2 gene. *Hum. Mol. Genet.* **19**, 4895–4905
52. Wevrick, R. (2020) Disentangling ingestive behavior-related phenotypes in Prader-Willi syndrome: Integrating information from nonclinical studies and clinical trials to better understand the pathophysiology of hyperphagia and obesity. *Physiol. Behav.* **219**, 112864
53. Lee, S., Kozlov, S., Hernandez, L., Chamberlain, S. J., Brannan, C. I., Stewart, C. L., and Wevrick, R. (2000) Expression and imprinting of MAGEL2 suggest a role in Prader-Willi syndrome and the homologous murine imprinting phenotype. *Hum. Mol. Genet.* **9**, 1813–1819
54. Chomez, P., De Backer, O., Bertrand, M., De Plaen, E., Boon, T., and Lucas, S. (2001) An overview of the MAGE gene family with the identification of all human members of the family. *Cancer Res.* **61**, 5544–5551
55. Marchler-Bauer, A., Bo, Y., Han, L., He, J., Lanczycki, C. J., Lu, S., Chitsaz, F., Derbyshire, M. K., Geer, R. C., Gonzales, N. R., Gwadz, M., Hurwitz, D. I., Lu, F., Marchler, G. H., Song, J. S., *et al.* (2017) CDD/SPARCLE: Functional classification of proteins via subfamily domain architectures. *Nucleic Acids Res.* **45**, D200–D203
56. Ludwig, A., and Krieger, M. A. (2016) Genomic and phylogenetic evidence of VIPER retrotransposon domestication in trypanosomatids. *Mem. Inst. Oswaldo Cruz* **111**, 765–769
57. Wood, J. D., Yuan, J., Margolis, R. L., Colomer, V., Duan, K., Kushi, J., Kaminsky, Z., Kleiderlein, J. J., Sharp, A. H., and Ross, C. A. (1998) Atrophin-1, the DRPLA gene product, interacts with two families of WW domain-containing proteins. *Mol. Cell. Neurosci.* **11**, 149–160
58. Wang, H., Hu, L., Dalen, K., Dorward, H., Marcinkiewicz, A., Russell, D., Gong, D., Londos, C., Yamaguchi, T., Holm, C., Rizzo, M. A., Brasaemle, D., and Sztalryd, C. (2009) Activation of hormone-sensitive lipase requires two steps, protein phosphorylation and binding to the PAT-1 domain of lipid droplet coat proteins. *J. Biol. Chem.* **284**, 32116–32125
59. Guruprasad, K., Reddy, B. V., and Pandit, M. W. (1990) Correlation between stability of a protein and its dipeptide composition: A novel approach for predicting *in vivo* stability of a protein from its primary sequence. *Protein Eng.* **4**, 155–161
60. Hanson, J., Paliwal, K. K., Litfin, T., and Zhou, Y. (2019) SPOT-Disorder2: Improved protein intrinsic disorder prediction by ensembled deep learning. *Genomics Proteomics Bioinformatics* **17**, 645–656
61. Tsang, B., Pritišanac, I., Scherer, S. W., Moses, A. M., and Forman-Kay, J. D. (2020) Phase separation as a missing mechanism for interpretation of disease mutations. *Cell* **183**, 1742–1756
62. Quiroz, F. G., and Chilkoti, A. (2015) Sequence heuristics to encode phase behaviour in intrinsically disordered protein polymers. *Nat. Mater.* **14**, 1164–1171
63. Bandziulis, R. J., Swanson, M. S., and Dreyfuss, G. (1989) RNA-binding proteins as developmental regulators. *Genes Dev.* **3**, 431–437
64. Vernon, R. M., Chong, P. A., Tsang, B., Kim, T. H., Bah, A., Farber, P., Lin, H., and Forman-Kay, J. D. (2018) Pi-Pi contacts are an overlooked protein feature relevant to phase separation. *Elife* **7**, e31486
65. Kozakova, L., Vondrova, L., Stejskal, K., Charalabous, P., Kolesar, P., Lehmann, A. R., Uldrijan, S., Sanderson, C. M., Zdrahal, Z., and Palecek, J. J. (2015) The melanoma-associated antigen 1 (MAGEA1) protein stimulates the E3 ubiquitin-ligase activity of TRIM31 within a TRIM31-MAGEA1-NSE4 complex. *Cell Cycle* **14**, 920–930
66. Oughtred, R., Rust, J., Chang, C., Breitkreutz, B. J., Stark, C., Willems, A., Boucher, L., Leung, G., Kolas, N., Zhang, F., Dolma, S., Coulombe-Huntington, J., Chatr-Aryamontri, A., Dolinski, K., and Tyers, M. (2021) The BioGRID database: A comprehensive biomedical resource of curated protein, genetic, and chemical interactions. *Protein Sci.* **30**, 187–200
67. Couzens, A. L., Knight, J. D., Kean, M. J., Teo, G., Weiss, A., Dunham, W. H., Lin, Z. Y., Bagshaw, R. D., Sicheri, F., Pawson, T., Wrana, J. L., Choi, H., and Gingras, A. C. (2013) Protein interaction network of the mammalian Hippo pathway reveals mechanisms of kinase-phosphatase interactions. *Sci. Signal.* **6**, rs15
68. Roux, K. J., Kim, D. I., and Burke, B. (2013) BioID: A screen for protein-protein interactions. *Curr. Protoc. Protein Sci.* **74**, 19.23.1–19.23.14
69. Kim, D. I., Birendra, K. C., Zhu, W., Motamedchaboki, K., Doye, V., and Roux, K. J. (2014) Probing nuclear pore complex architecture with proximity-dependent biotinylation. *Proc. Natl. Acad. Sci. U. S. A.* **111**, E2453–E2461
70. Mellacheruvu, D., Wright, Z., Couzens, A. L., Lambert, J. P., St-Denis, N. A., Li, T., Miteva, Y. V., Hauri, S., Sardiu, M. E., Low, T. Y., Halim, V. A., Bagshaw, R. D., Hubner, N. C., Al-Hakim, A., Bouchard, A., *et al.* (2013) The CRAPome: A contaminant repository for affinity purification-mass spectrometry data. *Nat. Methods* **10**, 730–736
71. Szklarczyk, D., Gable, A. L., Lyon, D., Junge, A., Wyder, S., Huerta-Cepas, J., Simonovic, M., Doncheva, N. T., Morris, J. H., Bork, P., Jensen, L. J., and Mering, C. V. (2019) STRING v11: Protein-protein association networks with increased coverage, supporting functional discovery in genome-wide experimental datasets. *Nucleic Acids Res.* **47**, D607–D613
72. Weidensdorfer, D., Stohr, N., Baude, A., Lederer, M., Kohn, M., Schierhorn, A., Buchmeier, S., Wahle, E., and Huttelmaier, S. (2009) Control of c-myc mRNA stability by IGF2BP1-associated cytoplasmic RNPs. *RNA* **15**, 104–115
73. Modelska, A., Turro, E., Russell, R., Beaton, J., Sbarrato, T., Spriggs, K., Miller, J., Graf, S., Provenzano, E., Blows, F., Pharoah, P., Caldas, C., and Le Quesne, J. (2015) The malignant phenotype in breast cancer is driven by eIF4A1-mediated changes in the translational landscape. *Cell Death Dis.* **6**, e1603

74. Shahbazian, D., Parsyan, A., Petroulakis, E., Hershey, J., and Sonenberg, N. (2010) eIF4B controls survival and proliferation and is regulated by proto-oncogenic signaling pathways. *Cell Cycle* **9**, 4106–4109
75. Soto-Rifo, R., Rubilar, P. S., and Ohlmann, T. (2013) The DEAD-box helicase DDX3 substitutes for the cap-binding protein eIF4E to promote compartmentalized translation initiation of the HIV-1 genomic RNA. *Nucleic Acids Res.* **41**, 6286–6299
76. Haspula, D., Vallejos, A. K., Moore, T. M., Tomar, N., Dash, R. K., and Hoffmann, B. R. (2019) Influence of a hyperglycemic microenvironment on a diabetic versus healthy rat vascular endothelium reveals distinguishable mechanistic and phenotypic responses. *Front. Physiol.* **10**, 558
77. Yang, J., Ren, B., Yang, G., Wang, H., Chen, G., You, L., Zhang, T., and Zhao, Y. (2020) The enhancement of glycolysis regulates pancreatic cancer metastasis. *Cell. Mol. Life Sci.* **77**, 305–321
78. Birge, R. B., Kalodimos, C., Inagaki, F., and Tanaka, S. (2009) Crk and CrkL adaptor proteins: Networks for physiological and pathological signaling. *Cell Commun. Signal.* **7**, 13
79. Zheng, C., Zheng, Z., Zhang, Z., Meng, J., Liu, Y., Ke, X., Hu, Q., and Wang, H. (2015) IFIT5 positively regulates NF-kappaB signaling through synergizing the recruitment of IkappaB kinase (IKK) to TGF-beta-activated kinase 1 (TAK1). *Cell Signal.* **27**, 2343–2354
80. Sakamoto, S., McCann, R. O., Dhir, R., and Kyprianou, N. (2010) Talin1 promotes tumor invasion and metastasis via focal adhesion signaling and anoikis resistance. *Cancer Res.* **70**, 1885–1895
81. O'Reilly, P. G., Wagner, S., Franks, D. J., Cailliau, K., Browaeys, E., Dissous, C., and Sabourin, L. A. (2005) The Ste20-like kinase SLK is required for cell cycle progression through G2. *J. Biol. Chem.* **280**, 42383–42390
82. Tang, M. K., Liang, Y. J., Chan, J. Y., Wong, S. W., Chen, E., Yao, Y., Gan, J., Xiao, L., Leung, H. C., Kung, H. F., Wang, H., and Lee, K. K. (2013) Promyelocytic leukemia (PML) protein plays important roles in regulating cell adhesion, morphology, proliferation and migration. *PLoS One* **8**, e59477
83. Kim, J., Kim, I., Yang, J. S., Shin, Y. E., Hwang, J., Park, S., Choi, Y. S., and Kim, S. (2012) Rewiring of PDZ domain-ligand interaction network contributed to eukaryotic evolution. *PLoS Genet.* **8**, e1002510
84. Zhou, H., Xu, Y., Yang, Y., Huang, A., Wu, J., and Shi, Y. (2005) Solution structure of AF-6 PDZ domain and its interaction with the C-terminal peptides from Neurexin and Bcr. *J. Biol. Chem.* **280**, 13841–13847
85. Bindea, G., Mlecnik, B., Hackl, H., Charoentong, P., Tosolini, M., Kirilovsky, A., Fridman, W. H., Pages, F., Trajanoski, Z., and Galon, J. (2009) ClueGO: A Cytoscape plug-in to decipher functionally grouped gene ontology and pathway annotation networks. *Bioinformatics* **25**, 1091–1093
86. Palecek, J. J., and Gruber, S. (2015) Kite proteins: A superfamily of SMC/Kleisin partners conserved across bacteria, archaea, and eukaryotes. *Structure* **23**, 2183–2190
87. Zabrady, K., Adamus, M., Vondrova, L., Liao, C., Skoupilova, H., Novakova, M., Jurcisinova, L., Alt, A., Oliver, A. W., Lehmann, A. R., and Palecek, J. J. (2016) Chromatin association of the SMC5/6 complex is dependent on binding of its NSE3 subunit to DNA. *Nucleic Acids Res.* **44**, 1064–1079
88. Sanderson, M. R., Badior, K. E., Fahlman, R. P., and Wevrick, R. (2020) The necdin interactome: Evaluating the effects of amino acid substitutions and cell stress using proximity-dependent biotinylation (BioID) and mass spectrometry. *Hum. Genet.* **139**, 1513–1529
89. Koval, A. P., Karas, M., Zick, Y., and LeRoith, D. (1998) Interplay of the proto-oncogene proteins CrkL and CrkII in insulin-like growth factor-I receptor-mediated signal transduction. *J. Biol. Chem.* **273**, 14780–14787
90. Karas, M., Koval, A. P., Zick, Y., and LeRoith, D. (2001) The insulin-like growth factor I receptor-induced interaction of insulin receptor substrate-4 and Crk-II. *Endocrinology* **142**, 1835–1840
91. Grosset, C., Chen, C. Y., Xu, N., Sonenberg, N., Jacquemin-Sablon, H., and Shyu, A. B. (2000) A mechanism for translationally coupled mRNA turnover: Interaction between the poly(A) tail and a c-fos RNA coding determinant via a protein complex. *Cell* **103**, 29–40
92. Lim, J., Ha, M., Chang, H., Kwon, S. C., Simanshu, D. K., Patel, D. J., and Kim, V. N. (2014) Uridylation by TUT4 and TUT7 marks mRNA for degradation. *Cell* **159**, 1365–1376
93. Valentin-Vega, Y. A., Wang, Y. D., Parker, M., Patmore, D. M., Kanagaraj, A., Moore, J., Rusch, M., Finkelstein, D., Ellison, D. W., Gilbertson, R. J., Zhang, J., Kim, H. J., and Taylor, J. P. (2016) Cancer-associated DDX3X mutations drive stress granule assembly and impair global translation. *Sci. Rep.* **6**, 25996
94. Habelhah, H., Shah, K., Huang, L., Ostareck-Lederer, A., Burlingame, A. L., Shokat, K. M., Hentze, M. W., and Ronai, Z. (2001) ERK phosphorylation drives cytoplasmic accumulation of hnRNP-K and inhibition of mRNA translation. *Nat. Cell Biol.* **3**, 325–330
95. Ye, J., Beetz, N., O'Keeffe, S., Tapia, J. C., Macpherson, L., Chen, W. V., Bassel-Duby, R., Olson, E. N., and Maniatis, T. (2015) hnRNP U protein is required for normal pre-mRNA splicing and postnatal heart development and function. *Proc. Natl. Acad. Sci. U. S. A.* **112**, E3020–E3029
96. Landthaler, M., Gaidatzis, D., Rothballer, A., Chen, P. Y., Soll, S. J., Dinic, L., Ojo, T., Hafner, M., Zavolan, M., and Tuschl, T. (2008) Molecular characterization of human Argonaute-containing ribonucleoprotein complexes and their bound target mRNAs. *RNA* **14**, 2580–2596
97. Lee, Y. J., Wei, H. M., Chen, L. Y., and Li, C. (2014) Localization of SERBP1 in stress granules and nucleoli. *FEBS J.* **281**, 352–364
98. Haque, N., Ouda, R., Chen, C., Ozato, K., and Hogg, J. R. (2018) ZFR coordinates crosstalk between RNA decay and transcription in innate immunity. *Nat. Commun.* **9**, 1145
99. Huang, C., Chen, Y., Dai, H., Zhang, H., Xie, M., Zhang, H., Chen, F., Kang, X., Bai, X., and Chen, Z. (2020) UBAP2L arginine methylation by PRMT1 modulates stress granule assembly. *Cell Death Differ.* **27**, 227–241
100. Youn, J. Y., Dunham, W. H., Hong, S. J., Knight, J. D. R., Bashkurov, M., Chen, G. I., Bagci, H., Rathod, B., MacLeod, G., Eng, S. W. M., Angers, S., Morris, Q., Fabian, M., Côté, J. F., and Gingras, A. C. (2018) High-density proximity mapping reveals the subcellular organization of mRNA-associated granules and bodies. *Mol. Cell* **69**, 517–532.e511
101. Wu, R., Li, A., Sun, B., Sun, J. G., Zhang, J., Zhang, T., Chen, Y., Xiao, Y., Gao, Y., Zhang, Q., Ma, J., Yang, X., Liao, Y., Lai, W. Y., Qi, X., *et al.* (2019) A novel m(6)A reader Prrc2a controls oligodendroglial specification and myelination. *Cell Res.* **29**, 23–41
102. Wang, X., Zhao, B. S., Roundtree, I. A., Lu, Z., Han, D., Ma, H., Weng, X., Chen, K., Shi, H., and He, C. (2015) N(6)-methyladenosine modulates messenger RNA translation efficiency. *Cell* **161**, 1388–1399
103. Patil, D. P., Pickering, B. F., and Jaffrey, S. R. (2018) Reading m(6)A in the transcriptome: m(6)A-binding proteins. *Trends Cell Biol.* **28**, 113–127
104. Zaccara, S., and Jaffrey, S. R. (2020) A unified model for the function of YTHDF proteins in regulating m(6)A-modified mRNA. *Cell* **181**, 1582–1595.e1518
105. He, P. C., and He, C. (2021) m(6) A RNA methylation: From mechanisms to therapeutic potential. *EMBO J.* **40**, e105977
106. Cho, H. J., Yu, J., Xie, C., Rudrabhatla, P., Chen, X., Wu, J., Parisiadou, L., Liu, G., Sun, L., Ma, B., Ding, J., Liu, Z., and Cai, H. (2014) Leucine-rich repeat kinase 2 regulates Sec16A at ER exit sites to allow ER-Golgi export. *EMBO J.* **33**, 2314–2331
107. Piao, H., Kim, J., Noh, S. H., Kweon, H. S., Kim, J. Y., and Lee, M. G. (2017) Sec16A is critical for both conventional and unconventional secretion of CFTR. *Sci. Rep.* **7**, 39887
108. Merte, J., Jensen, D., Wright, K., Sarsfield, S., Wang, Y., Schekman, R., and Ginty, D. D. (2010) Sec24b selectively sorts Vangl2 to regulate planar cell polarity during neural tube closure. *Nat. Cell Biol.* **12**, 41–46. sup pp 41-48
109. Jassal, B., Matthews, L., Viteri, G., Gong, C., Lorente, P., Fabregat, A., Sidiropoulos, K., Cook, J., Gillespie, M., Haw, R., Loney, F., May, B., Milacic, M., Rothfels, K., Sevilla, C., *et al.* (2020) The reactome pathway knowledgebase. *Nucleic Acids Res.* **48**, D498–D503
110. Goldstrohm, A. C., Hall, T. M. T., and McKenney, K. M. (2018) Post-transcriptional regulatory functions of mammalian Pumilio proteins. *Trends Genet.* **34**, 972–990

111. Miller, S. E., Collins, B. M., McCoy, A. J., Robinson, M. S., and Owen, D. J. (2007) A SNARE-adaptor interaction is a new mode of cargo recognition in clathrin-coated vesicles. *Nature* **450**, 570–574
112. Aumais, J. P., Tunstead, J. R., McNeil, R. S., Schaar, B. T., McConnell, S. K., Lin, S. H., Clark, G. D., and Yu-Lee, L. Y. (2001) NudC associates with Lis1 and the dynein motor at the leading pole of neurons. *J. Neurosci.* **21**, RC187
113. Baillat, D., and Shiekhattar, R. (2009) Functional dissection of the human TNRC6 (GW182-related) family of proteins. *Mol. Cell. Biol.* **29**, 4144–4155
114. Goss, D. J., and Kleiman, F. E. (2013) Poly(A) binding proteins: Are they all created equal? *Wiley Interdiscip. Rev. RNA* **4**, 167–179
115. Huntzinger, E., Braun, J. E., Heimstädt, S., Zekri, L., and Izaurralde, E. (2010) Two PABPC1-binding sites in GW182 proteins promote miRNA-mediated gene silencing. *EMBO J.* **29**, 4146–4160
116. Fei, Q., Zou, Z., Roundtree, I. A., Sun, H. L., and He, C. (2020) YTHDF2 promotes mitotic entry and is regulated by cell cycle mediators. *PLoS Biol.* **18**, e3000664
117. Ries, R. J., Zaccara, S., Klein, P., Olarerin-George, A., Namkoong, S., Pickering, B. F., Patil, D. P., Kwak, H., Lee, J. H., and Jaffrey, S. R. (2019) m(6)A enhances the phase separation potential of mRNA. *Nature* **571**, 424–428
118. Zhou, J., Wan, J., Gao, X., Zhang, X., Jaffrey, S. R., and Qian, S. B. (2015) Dynamic m(6)A mRNA methylation directs translational control of heat shock response. *Nature* **526**, 591–594
119. Suzuki, K., Bose, P., Leong-Quong, R. Y., Fujita, D. J., and Riabowol, K. (2010) REAP: A two minute cell fractionation method. *BMC Res. Notes* **3**, 294
120. Li, X., Hughes, S. C., and Wevrick, R. (2015) Evaluation of melanoma antigen (MAGE) gene expression in human cancers using the Cancer Genome Atlas. *Cancer Genet.* **208**, 25–34
121. Fu, Y., and Zhuang, X. (2020) m(6)A-binding YTHDF proteins promote stress granule formation. *Nat. Chem. Biol.* **16**, 955–963
122. Banani, S. F., Lee, H. O., Hyman, A. A., and Rosen, M. K. (2017) Biomolecular condensates: Organizers of cellular biochemistry. *Nat. Rev. Mol. Cell Biol.* **18**, 285–298
123. Decker, C. J., and Parker, R. (2012) P-bodies and stress granules: Possible roles in the control of translation and mRNA degradation. *Cold Spring Harb. Perspect. Biol.* **4**, a012286
124. Florke Gee, R. R., Chen, H., Lee, A. K., Daly, C. A., Wilander, B. A., Fon Tacer, K., and Potts, P. R. (2020) Emerging roles of the MAGE protein family in stress response pathways. *J. Biol. Chem.* **295**, 16121–16155
125. Quesnel-Vallières, M., Weatheritt, R. J., Cordes, S. P., and Blencowe, B. J. (2019) Autism spectrum disorder: Insights into convergent mechanisms from transcriptomics. *Nat. Rev. Genet.* **20**, 51–63
126. Stepanenko, A. A., and Dmitrenko, V. V. (2015) HEK293 in cell biology and cancer research: Phenotype, karyotype, tumorigenicity, and stress-induced genome-phenotype evolution. *Gene* **569**, 182–190
127. Erickson, H. P. (2009) Size and shape of protein molecules at the nanometer level determined by sedimentation, gel filtration, and electron microscopy. *Biol. Proced. Online* **11**, 32–51
128. Berman, H. M., Westbrook, J., Feng, Z., Gilliland, G., Bhat, T. N., Weissig, H., Shindyalov, I. N., and Bourne, P. E. (2000) The Protein Data Bank. *Nucleic Acids Res.* **28**, 235–242
129. Troshin, P. V., Procter, J. B., Sherstnev, A., Barton, D. L., Madeira, F., and Barton, G. J. (2018) JABAWS 2.2 distributed web services for bioinformatics: Protein disorder, conservation and RNA secondary structure. *Bioinformatics* **34**, 1939–1940
130. Lancaster, A. K., Nutter-Upham, A., Lindquist, S., and King, O. D. (2014) PLAAC: A web and command-line application to identify proteins with prion-like amino acid composition. *Bioinformatics* **30**, 2501–2502
131. Shi, H., Wang, X., Lu, Z., Zhao, B. S., Ma, H., Hsu, P. J., Liu, C., and He, C. (2017) YTHDF3 facilitates translation and decay of N(6)-methyladenosine-modified RNA. *Cell Res.* **27**, 315–328
132. Lambert, J. P., Tucholska, M., Go, C., Knight, J. D., and Gingras, A. C. (2015) Proximity biotinylation and affinity purification are complementary approaches for the interactome mapping of chromatin-associated protein complexes. *J. Proteomics* **118**, 81–94
133. Gupta, G. D., Coyaud, E., Goncalves, J., Mojarad, B. A., Liu, Y., Wu, Q., Gheiratmand, L., Comartin, D., Tkach, J. M., Cheung, S. W., Bashkurov, M., Hasegan, M., Knight, J. D., Lin, Z. Y., Schueler, M., *et al.* (2015) A dynamic protein interaction landscape of the human Centrosome-Cilium interface. *Cell* **163**, 1484–1499
134. Bush, J. R., and Wevrick, R. (2008) The Prader-Willi syndrome protein necdin interacts with the E1A-like inhibitor of differentiation EID-1 and promotes myoblast differentiation. *Differentiation* **76**, 994–1005